Test of Particle Identification at Target Rapidity in the E814 Experiment

Roger Lacasse

Physics Department

McGill University, Montréal

A thesis submited to the Faculty

of Graduate Studies and Research

in partial fulfillment of the requirements

for the Degree of Master of Science.

December 1991

Abstract

One of the unique features of the E814 experimental setup at the BNL-AGS, is its nearly 4π calorimetry. Calorimeters, however, do not provide information on the nature of particles and their multiplicity. Particle identification is important to understand the expansion phase of the hot nuclear matter produced in relativistic heavy ion collisions In the present 814 experiment the charged particle multiplicity is measured, at forward angles only, by a Si pad detector. The addition of a similar Si detector in the target rapidity region, overlapping the Target Calorimeter, is being considered. Initial calculations have shown a possibility of particle identification by using the signals from a silicon detector and from the highly segmented Target Calorimeter. In this thesis, the potential for particle identification of an upgraded silicon multiplicity detector at target rapidity is evaluated using a silicon surface barrier detector and part of the Target Calorimeter. The measured response is compared to the predictions of the event generator HIJET followed by complete tracking using the code GEANT.

Résumé

L'expérience E814 à l'AGS du BNL possède la particularité d'avoir une couverture calorimétrique de presque 4π. Les calorimetres, en général, ne fournissent pas d'information sur la nature des particules, ni sur leur multiplicité L'identification des particules est importante pour la compréhension de la phase d'expansion de la matière nucléaire chaude qui est produite au cours des collisions d'ions lourds relativistes Dans cette expérience, la multiplicité des particules chargées n'est mesurée qu'aux angles avants avec un détecteur au silicium. L'addition d'un détecteur au silicium, semblable à celui existant, aux rapidités de la cible est considérée de façon à couvrir le même domaine angulaire que le "Target Calorimeter" Des calculs préliminaires ont indiqué qu'il serait possible d'identifier les particules en utilisant les signaux d'un détecteur au silicium et ceux du "Target Calorimeter" Cette thèse étudie la qualité de l'identification de particules qui serait ainsi obtenue à l'aide d'un détecteur au silicium à barrière de surface et une partie du "Target Calorimeter". Les résultats de ce test sont comparés aux prédictions faitent par le générateur d'évenements HIJET après simulation de la réponse des détecteurs avec l'algorithme GEANT.

To my parents and

their unconditional support

Contents

List of Figures

Acknowledgements

I am most grateful to Dr Jean Barrette, my advisor His comprehensive knowledge and personal insight have been of great benefit to me during my studies This work would not have been possible without his confidence and support

I express my gratitude to Dr Claude Pruneau As a neophyte, I tested his patience on many occasions and it never failed I also want to thank Dr S K Mark and his unalterable optimism

I appreciate the time that Dave Lunney took off his own thesis writing to read the manuscript I am also obliged to Francine Morrier for the final assembly of this document

Many thanks to all my collaborators on the 814 experiment and all the staff at the Foster Radiation Laboratory for providing a wonderful working environment

Finally, I thank my wife for her love and support during all the difficult times of a graduate student's life

Roger Lacasse

1

Introduction

1.1 Relativistic Heavy Ion Collisions

Since 1986, nuclear beams accelerated to energies E > 10 GeV/c/A have been available at BNL's AGS (Brookhaven National Laboratory's Alternate Gradient Synchrotron) and at CERN's SPS (Centre Européen de Recherche Nucléaire Super Proton Synchrotron) These Relativistic Heavy Ion (RHI) beams are used to study nuclear matter at high temperature and density with the hope of eventually finding evidence of a new phase of nuclear matter the Quark-Gluon Plasma (QGP)

Quantum Chromodynamic (QCD) lattice Monte Carlo calculations predict that the QGP would be formed at temperatures of T > 160 MeV † and at energy densities of $\rho_E > 1$ GeV/fm^3 It would have a lifetime of the order of $t \approx 10^{-23}$ s [RA82]. There is a possibility to produce this phase transition even at beam energies as low as 10 to 20 GeV/A [NA88] However, the dynamics of the nucleus-nucleus collision has to allow the deposition of enough energy in the fireball to reach the requisite conditions for the creation of the QGP. The answer to this question is intimately related to the notions of transparency and stopping power of hot nuclear matter. Experimentally measured transverse energy and forward nucleon spectra demonstrate that large energy depositions (full stopping) are observed for heavy targets at the AGS [BA90A] Large amounts of stopping with heavy targets are also observed at CERN.

† 1 eV = 1 602 × 10^{-19} J

To determine whether or not a new phase of matter is experimentally observed, one may look for unusual phenomena which would be characteristic of a QGP Transverse energy spectra (dE_t/dy) and rapidity distributions of particles (dN/dy) have been investigated for anomalous effects but nothing peculiar has been found [JA89] †

In a QGP, the effective strange quark mass is predicted to be much lighter than in a hadron gas so that the strangeness content would be strongly enhanced [FR89] Unusually high experimental K/π ratios have in fact been observed [AB90] However, it is still not clear if it is due to the formation of a QGP or to more conventional processes like rescattering of the reaction products (π^+) which could provide an alternative mechanism for K^+ enhancement At higher energies, a substantial reduction of the J/ψ yield was expected to provide a signature of the formation of a QGP [MA86] However, it is now understood that absorption by the very dense nuclear matter can produce a similar effect [SA89] The observation of exotica such as Strangelets, hadron bags of many quarks including many strange quarks which might be stable [WI84], could also provide evidence of the formation of a new state of nuclear matter Searches for strangelets have been conducted and upper limits have been obtained for the production of these postulated phenomena at AGS energies [BA90C]

Currently, no unambiguous signature of the formation of a QGP has been observed Whether the studied systems have undergone a phase transition is still an unsettled issue [ST91]. However, there are indications that the normal properties of nuclear matter are altered at high energy densities. A better understanding of the reaction dynamics is needed to identify exotic phenomena like the transition to a QGP Global observables, such as transverse energy and charged particle production, are used to characterize the centrality of the reactions [TI88] They also provide information on the amount of stopping achieved Information on the temperature of the fireball and on the entropy production can be obtained from the transverse momentum spectra of identified particles With particle identification, information on the magnitudes of the chemical potentials inside the fireball is obtained from the relative abundances of each

† The rapidity of a particle is defined as $y \equiv \frac{1}{2}\ln\left(\frac{E+p_z}{E-p_z}\right)$ where E is its energy and p_z, its momentum component along the beam direction

particle type. It also allows to make measurements in terms of rapidity rather than pseudorapidity ‡ (η) which is important at AGS energies because of the lower average energies of the particles.

1.2 Proposed Upgrade of the E814 Setup

One of the unique features of the experiment 814 (E814) at BNL is its nearly 4π calorimetric coverage surrounding the target. A schematic layout of the E814 setup is given in figure 2.1 Highly segmented calorimeters provide energy and pseudorapidity (or position) measurements but do not give sufficient information to allow particle identification. The identification of particles requires sets of at least two measurements such as energy and momentum, velocity and momentum or energy loss rate and total energy.

E814 has a multiplicity detector covering $2° < \theta < 30°$ as shown in figure 2.1. It is made of two silicon pad detectors which are sensitive to charged particles. It measures charged particle multiplicity and distribution (dN_c/dy). For heavy targets, the dN_c/dy distribution measurement is limited to the forward region in the center of mass. As part of a scheduled upgrade of the E814 setup, the extension of the charged particle multiplicity measurement to backward angles is being considered. This extended multiplicity detector would cover the target region where rescattering effects would dominate In addition to the dN_c/dy measurement, one could get an energy loss rate (dE/dx) measurement by digitalizing the amplitude of the signals from the extended multiplicity detector. A measurement of the total energy (E) of the particles emitted at near target rapidities is already available from the E814 target calorimeter. By correlating the E and dE/dx information, one would get a simple telescope detector that could provide some particle identification at target rapidities. The objective of this thesis is to test the quality of the particle identification that is achievable with the simple addition of a silicon detector in front of the existing E814 target calorimeter. Two particle identification methods are proposed in the next section.

‡ Pseudorapidity is defined as $\eta \equiv -\ln\tan(\theta/2)$

1.3 Particle Identification

An initial study of the quality of the particle identification that can be achieved with the proposed upgrade of the E814 experimental setup is presented here. Two methods of particle identification are studied in the two following subsections. The first method uses the information from a silicon detector only to achieve particle identification while the second method correlates the information of a silicon detector with the energy measurement from a calorimeter.

One of the numerous techniques which has been devised for particle identification uses Detector Telescopes [GO75] First reported in 1958 [GO79], telescopes have been made in a variety of forms over the years depending on the range of energies that are to be measured and types of particles to be identified [DE63] [FA87] The general technique consists of using several detectors of different thicknesses to measure the differential rates of energy loss and the total energy of the particles.

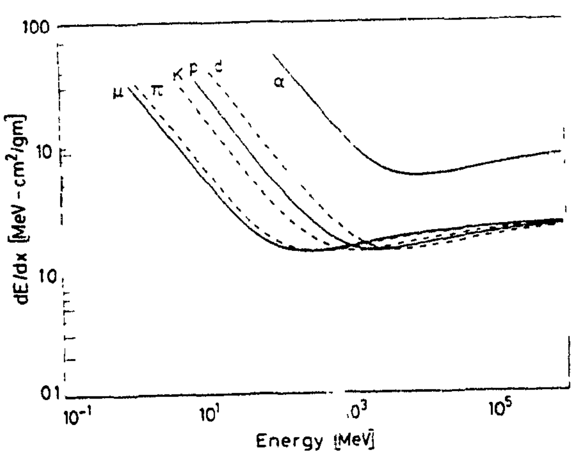

figure 1.1 Energy loss rates. The stopping power dE/dx is plotted as a function of energy for different particles.

The rate of energy loss of a particle in matter is approximatively given by the Bethe-Bloch formula [HE90]. It is plotted in figure 1.1 for various particles as a function of the particle's energy [LE87]. At low energies, the specific energy loss decreases as $1/\beta$ whereas at relativistic energies it reaches a minimum of $dE/dx \approx 1.5$ MeV cm^2/g in silicon. At the larger energies, the rates of energy loss increase logarithmically with

γ * Particles with energies past the minimum ($\gamma > 4$) are called Minimum Ionizing Particles (MIP) and can't be distinguished on the basis of dE/dx alone. Bellow this level, the measurement of dE/dx and of E uniquely defines the particle type. The most abundant particles produced at target rapidities in RHI collisions are pions and protons Their average energies are of the order of 1 GeV [WA90]. Therefore, most of the pions are MIP whereas most of the protons are not. It should be possible to distinguish particles on the basis of dE/dx and E measurements made with a telescope detector.

1.3.1 Identification with a silicon detector

For high energy fixed target experiments there is a strong correlation between the average particle energy and angular direction. In the forward angle region ($\theta < 45°$), most emitted particles have energies from a few GeV to 14 GeV because of the high velocity of the center of mass. Therefore, they are mainly minimum ionizing. They are thus impossible to identify using a simple dE/dx measurement. At backward angles however, particles get softer, protons become more ionizing than the pions thereby allowing particle identification based on the dE/dx information alone.

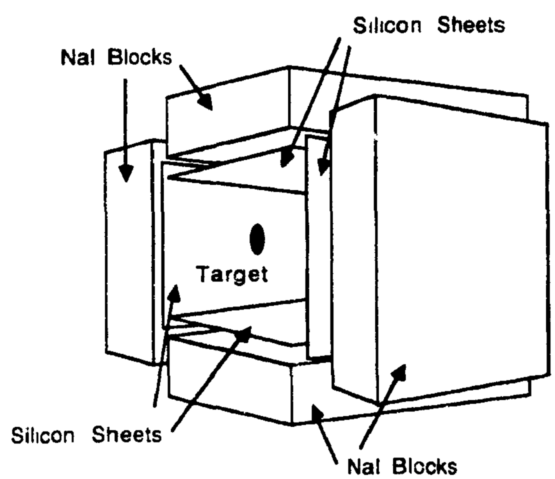

Figure 1.2 Simple model of the experimental setup for particle identification evaluation (not drawn to scale).

* $\gamma = (1 - \beta^2)^{-1/2}$, $\beta = v/c$

Model calculations were made in order to find the angular region where the proportion of protons is important and to determine where kinematics allow particle identification with the first method. The simulation uses the HIJET event generator and particles are tracked using the program GEANT both of which are discussed in section 4.1. The experimental setup was simulated using a simplified description of the detectors as shown in figure 1.2. It assumes four sheets of silicon 300 μm thick surrounding the target and four large blocks of NaI with the same thickness as the E814 target calorimeter (see section 2.1.2). The detectors cover the angular range $55° < \theta < 135°$. The simulation starts by generating the particles with HIJET at the position of the target. The particles are then tracked, one at a time, through the detectors by GEANT. Because of the large angular range used in this simplified simulation, the energy losses are corrected to take into account the change in thickness with incident angle. The contributions of the particles are integrated over different angular ranges to increase statistics. Here, it is assumed that no strong variations in the rapidity distributions occur within these angular ranges.

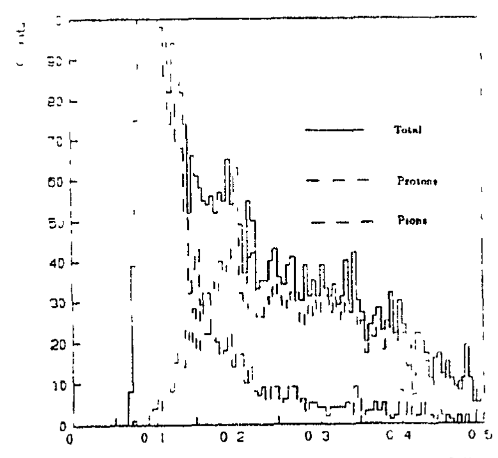

Figure 1.3 Energy loss of protons and pions in a 300 μm thick silicon detector. A summation over the angular range of $75° < \theta < 135°$ is made.

The calculated energy loss spectra for p and π in the silicon sheets is plotted in figure 1.3 for the backward angles ($75° < \theta < 135°$). According to the event generator, most of the minimum ionizing peak, around 100 KeV, consists of π while most of the p have larger energy losses. One can evaluate the quality of particle identification using the silicon detector alone by defining the numbers of particles above $N_>$ and below $N_<$ an arbitrary cut as given by:

$$\begin{aligned} N_< &= n_p^< + n_\pi^< \\ N_> &= n_p^> + n_\pi^> \end{aligned} \tag{1.1}$$

The terms on the right side of equation (1.1) can be expressed as·

$$\begin{aligned} n_p^< &= f_p^< n_p, \qquad & n_p^> &= f_p^> n_p \\ n_\pi^< &= f_\pi^< n_\pi, \qquad & n_\pi^> &= f_\pi^> n_\pi \end{aligned} \tag{1.2}$$

where n_π and n_p are the number of particles of each type. $f_i^>$ and $f_i^<$ are the fraction of particles above and below the cut and are normalized so that:

$$f_i^< + f_i^> = 1 \tag{1.3}$$

Expression (1.1) can now be rewritten in matrix notation as:

$$\begin{pmatrix} N_< \\ N_> \end{pmatrix} = \begin{pmatrix} f_p^< & f_\pi^< \\ f_p^> & f_\pi^> \end{pmatrix} \begin{pmatrix} n_p \\ n_\pi \end{pmatrix} \tag{1.4}$$

Inverting the relationship (1.4) gives:

$$\begin{pmatrix} n_p \\ n_\pi \end{pmatrix} = \frac{1}{\Delta} \begin{pmatrix} f_\pi^> & -f_\pi^< \\ -f_p^> & f_p^< \end{pmatrix} \begin{pmatrix} N_< \\ N_> \end{pmatrix} \tag{1.5}$$

where:

$$\Delta = f_\pi^> f_p^< - f_\pi^< f_p^> .$$

This simple method has three steps. First, the f coefficients are calculated from a theoretical model. Then, the values of $N_<$ and $N_>$ are obtained from the data. Finally, one gets the value of the ratio p/π using formula (1.5). To test the particle identification the cut is selected at 0.150 MeV where the predicted contributions of each type of particle are nearly equal. Using this threshold, the average value of the f coefficients above the cut are given in table 1.1 for three angular ranges.

As expected the fraction $f_p^>$ increases with angle because of the reduced average energy of the particles. In the angular range $75° < \theta < 135°$, it is predicted that 92% of the protons would give signals above threshold. The fraction of pions $f_\pi^>$ is small but it also increases with angle. This will result in a reduced precision in the particle identification, however, this increase in $f_\pi^>$ is relatively slow. The calculated ratio of

Angular Range (degrees)	$f_\pi^<$	$f_\pi^>$	$f_p^<$	$f_p^>$	p/π
55 - 65	0.76	0.24	0.21	0.79	1.06
65 - 75	0.74	0.26	0.15	0.85	1.06
75 - 135	0.72	0.28	0.07	0.93	0.97

Table 1.1 p/π ratio estimates for three angular ranges made with HIJET and tracked by GEANT for central collisions of $^{28}Si + ^{208}Pb$ at 14 GeV/A

the number of protons to the number of pions produced in the reaction is given in the last column of the table. It is relatively constant over the angular range considered

1.3.2 Identification with a Si-NaI telescope

In the previous section it is shown that the energy loss can be use to determine roughly the relative number of p and π This method has the disadvantage of being model dependant. The f coefficients are obtained from energy loss spectra calculated for particles generated according to a theoretical model. Therefore, their values might change somewhat with the various models and as a result the deduced numbers of p and π. However, a model independent measurement of the p/π ratio is possible by combining a measurement of the residual energy to the energy loss obtained in a silicon detector. Such a combination is called a telescope detector system

To evaluate the expected performance of such a telescope, the initial simulations were done by assuming an infinitely thick NaI detector behind the silicon sheet A more realistic simulation was also done with a 13.8 cm thick NaI detector which is close to the average thickness of the E814 target calorimeter (TCAL). In the simulation, both NaI detectors are large single blocks covering the entire angular range of the silicon sheets.

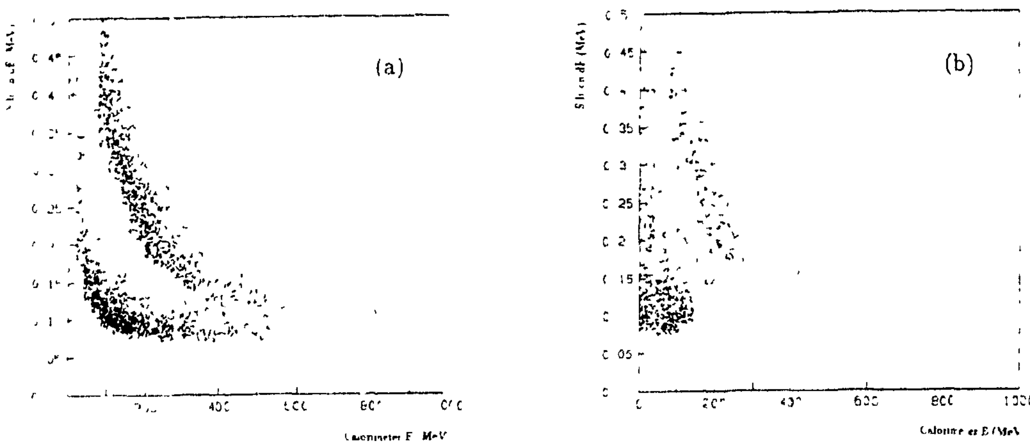

Figure 1.4 dE vs E for a 300 μm thick silicon detector. (a) dE in a 300μ thick silicon detector vs total E deposited in an infinitely thick NaI calorimeter. (b) dE vs E loss in a NaI block

A scatter plot of the calculated dE vs E signals of π's and p's with an infinitely thick calorimeter is shown in figure 1.4(a). Particles of low energy leave a large dE signal in the silicon detector and a small total E signal in the calorimeter. For particles with higher energies, the dE signal decreases as the total E detected increases. Sufficiently energetic particles all leave similar signals in the silicon detector but the total energy detected continues to increase. In agreement with figure 1.1, one also see that p's and π's are minimum ionizing at different total energy So, identification is possible even if particles are minimum ionizing in the silicon detector.

The E814 target calorimeter is not infinitely thick and energetic particles punch through it. In such cases, the total energy of the particles is not measured anymore. Figure 1.4(b) shows the expected response from a more realistic detector with a finite thickness. Above a maximal energy of $\sim$ 200 MeV, the energy loss in the calorimeter decreases. A sufficiently high momentum proton ends up in the same region as the minimum ionizing high energy pions. However, this overlap is relatively small and can be partly accounted for by extrapolating from the lower momentum spectra. The results from this initial simulation thus indicates that by using the energy information one expects a resonable separation of p and π.

In conclusion, the main goal of this thesis is to study the possibility of achieving particle identification at target rapidities with the addition of a silicon barrier detector to the existing E814 experimental setup This is done particularly with the objective of measuring the p/π ratio at target rapidities The E814 experimental setup and the setup used to perform the present test are described in chapter 2 Descriptions of the data analysis programs and of the measurements are given in chapter 3 Extensive Monte Carlo calculations are presented in chapter 4 to understand the experimental data. The test results are summarized in the conclusion.

2

Experimental Setup

2.1 The E814 Setup

The E814 collaboration has a threefold physics program for the study of relativistic heavy ions collisions:

- The investigation of central collisions by energy and transverse momentum flow analysis and correlation with the leading projectile fragments detected in the forward spectrometer; this provides information on reaction mechanisms leading to hot nuclear matter at high energy density [BA90A].

- The study of peripheral collisions and the effects of the relativistically enhanced Coulomb field of the target on the projectile. This is done by identification and tracking of all the projectile's fragments [BA90B].

- A search for metastable massive multiquark states of strange matter made plausible on the basis of the Pauli exclusion principle [BA91C].

In order to cover this wide range of physics, the E814 setup is built with complete 4π calorimeter coverage around the target region and is complemented with a high resolution forward spectrometer along the beam direction. In the following pages an overview of all the E814 setup is given. A much more exhaustive description of the E814 spectrometer can be found in the experiment proposal document [LI86] or in reference [BA90B].

The E814 experimental setup is illustrated on figure 2.1. It is divided into two groups, the upstream and downstream sets The downstream set or forward magnetic spectrometer is composed of two dipole magnets (M1,M2), the tracking chambers (DC1,DC2,DC3), uranium calorimeters (UCAL), forward scintillators (FSCI) and the magnet scintillators (MSCI) This set was not directly used in the present test but the experimental trigger (late timing trigger) is based on some of its detectors The upstream set, covering almost 4π in solid angle, is made of the target calorimeters (TCAL), target scintillators paddles (TPAD), participant calorimeter (PCAL) and the silicon multiplicity detector (MULT).

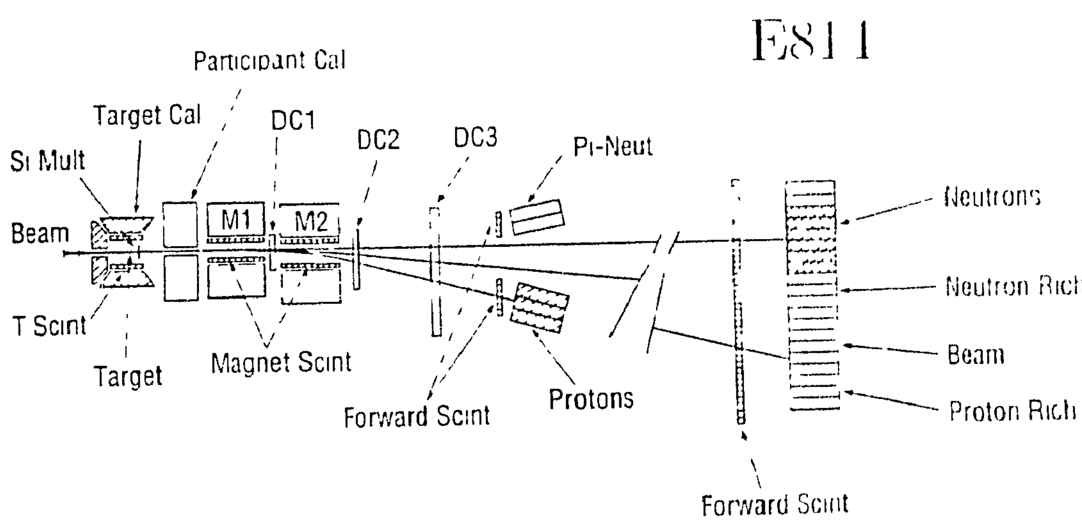

Figure 2.1 The E814 experimental setup. It is divided into two groups the forward spectrometer and the upstream set. Solid lines on the figure represent trajectories for neutral particles, beamlike particles (with $Z/A = 1/2$) and protons with 14.6 GeV/A momentum for the maximum field of 3 T.

2.1.1 Forward Magnetic Spectrometer

The downstream group of detectors is usually referred to as the forward spectrometer. It is used to determine the charge, momentum and energy of the particles that go through the central opening of the participant calorimeter This opening forms a cone of approximatively $0.8°$ centered on the beam axis. The particles traverse two dipole magnets (M1,M2) with an integrated magnetic flux of 6 T·m Pions produced in grazing collisions are detected by the 16 magnet scintillators lining the inside walls of the two magnets.

Three tracking chambers (labelled DC1, DC2 and DC3 in figure 2 1) are used to determine the charged particle momenta The first drift chamber (DC1) is located in between the the two magnets M1 and M2 It consists of a pad plane whose readout provides a measure of vertical position of the charged particle tracks The two other drift chambers (DC2,DC3) are located downstream of the magnets Both are made of 6 wire planes and 1 pad plane The drift chambers allow the simultaneous measurement of the position in two dimensions of many particles The six wire planes provide an accurate measure of the horizontal position and a rough estimate of the particle directions The pad planes are used to determine the vertical position of the tracks The magnetic rigidity (p/Z) of each particle is obtained from the radius of curvature determined by track reconstruction using the information from the three chambers

The drift chamber tracking is complemented with a time of flight (TOF) and energy measurement. The charged particle TOF measurement is accomplished with an hodoscope of 58 narrow vertical slats of scintillator Each scintillator measures $10 \times 120 \times 1$ cm^3. Each slat of the forward scintillators (FSCI) is viewed at each end by a phototube. The energy of both charged and neutral particles is measured with 25 uranium calorimeters (UCAL) modules. Each calorimeter has a cross sectional area of 20×120 cm^2 and is read out in optically decoupled towers of 10×20 cm^2 The FSCI and UCAL are split into three groups. Two of these are located right behind DC3 12 m from the target. One group is used for the search of postulated collective states of pions and neutrons (Pi-Neut). The other group is placed on the proton (Protons) side and is used to measure their energy and TOF. The third group is positioned 36 m from the target. The uranium calorimeters are discussed in detail in reference [FA91].

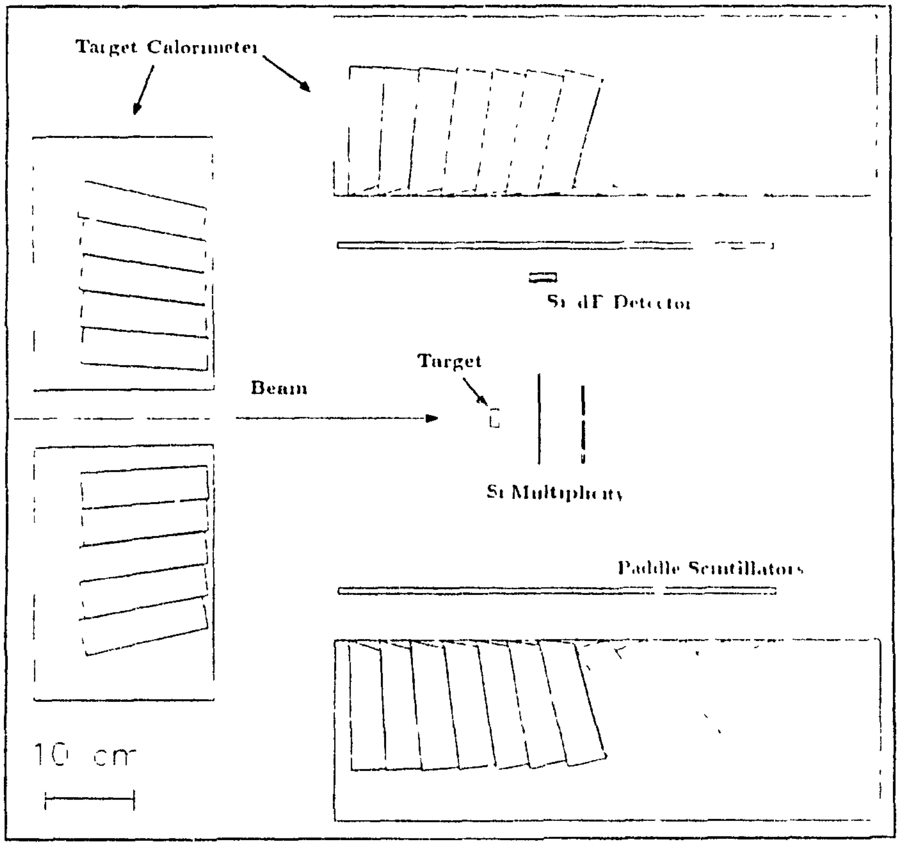

Figure 2.2 Side view of the target region of the E814 experiment It is viewed perpendicularly to the beam axis. The Silicon detector is shown to scale, in its position and orientation.

2.1.2 Upstream Set of the E814 Detectors

The detectors surrounding the target region and the silicon barrier detector used for the present test are shown in more detail in figure 2.2. A set of two silicon pad detectors, called the multiplicity detector (MULT), is placed right after the target This combination of two detectors covers the angular range of $2^\circ < \theta < 30^\circ$ or, in terms of pseudorapidity, $1.3 < \eta < 4.0$ The two detectors are 300 μm thick Si wafers 76 mm in diameter which are sensitive to the passage of charged particles They are each segmented radially and azimuthally into 512 pads. They are used to measure the multiplicity of charged particles produced in the collisions A detailed description is given in [BA91B]

An important feature of the E814 setup is its quasi-4π calorimetric coverage around the target This is achieved with two distinct calorimeters The first detector, the participant calorimeter (PCAL) (not shown in figure 2.2), is a lead glass wall which covers roughly the same angular range as the multiplicity detector ($2^\circ < \theta < 45^\circ$) It is a sampling calorimeter made of lead and scintillator plates The PCAL is divided into four quadrants read by optical fibers connected to phototubes Each quadrant includes 28 towers which are divided longitudinally into two electromagnetic and two hadronic sections with a total thickness of 4 nuclear interaction lengths

The reaction fragments emitted at angles greater than 45° are detected in the target calorimeter (TCAL) It is sensitive to charged and neutral particles as well as gamma rays The TCAL is made of 992 NaI crystals roughly 13.8 cm long and with a cross section of 2.5×2.5 cm^2 Their thickness corresponds to 5 3 radiation lengths or 1/3 of a nuclear interaction length. The crystals are mounted in a quasi projective geometry as illustrated in figure 2 1 They are positioned into five walls. Four walls are parallel and one is perpendicular to the beam axis They cover, respectively, $45^\circ < \theta < 118^\circ$ ($-0.5 < \eta < 0.8$) and $135^\circ < \theta < 165^\circ$ ($-2.0 < \eta < -0.9$) The crystals are individually read by a vacuum photodiode. The average noise in a channel corresponds to a standard deviation of $\sigma_E = 1.5$ MeV The energy calibration is performed over a period of several weeks using cosmic rays. A detailed description of the construction, testing, energy calibration and operation of this detector is given in reference [WA90].

The transverse energy production (E_t)[TI88] is measured with both the PCAL and the TCAL Generally, E_t is used as a measure of energy deposition and of collision centrality In this work, the E_t measured with the TCAL is used to correct for trigger bias. This correction is discussed in section 4 3.

The inner walls of the target calorimeter are lined with 52 plastic scintillators arranged parallel to the beam The target paddle detectors (TPAD) are each viewed by a single phototube They are used online in the data acquisition to provide an approximate measure of the charged particle multiplicity. Since the TPAD stretches from the front to the back of the TCAL the probability for two particles to hit the same detector (double hits) is very high Therefore, they are not used in the present analysis. However, they were included as dead material in the simulations described chapter 4 since their thickness is not negligible

2.2 The Silicon Detector Setup

The Silicon detector was installed inside the target calorimeter as shown on figure 2 2 It was positioned above the beam axis at an angle of $\sim 70°$ The distance from the detector to the target is 16 5 cm It covers a solid angle of $\Omega = 0\ 011$ sr between $68° < \theta < 72°$ $(0\ 28 < \eta < 0\ 40)$

For the test, a fully depleted silicon surface barrier detector was used. The detector was made by Tennelec It has a thickness of 510 μm with an active area of 300 mm^2 At the operating bias of 230 V the measured leakage current was 0 46 μA No appreciable increase of the leakage current was observed over the running time The nominal resolution specified by Tennelec [TE90] is 19 keV FWHM† for the 5 486 MeV ^{241}Am α line. Before its installation in the E814 setup, the width of this line was measured with the silicon detector to have a standard deviation $\sigma \approx 14$ keV or 32 keV FWHM at the shaping amplifier level which is consistent with the nominal resolution.

2.3 Electronics

A schematic representation of the silicon detector electronics used in the present test is given in figure 2 3 The detector was connected through a single 20 cm microdot cable to an Ortec 109A preamplifier The detector bias was supplied by an Ortec 210 four-channel silicon detector power supply The preamplifier output signal was sent to a Canberra shaping amplifier which also supplied power to the preamplifier The shaping amplifier normalized bipolar signals (with a shaping time of 250 ns) were sent through a 100 m cable to a LeCroy 2249W Analog-to-Digital Converter (ADC) installed in the E814 counting house The 2249W is a 12-channel 11 bit charge integrating ADC with a sensitivity of 25 pC per channel Given the shape of the signals from the amplifier,

† Full Width at Half the Maximum = 2 35σ

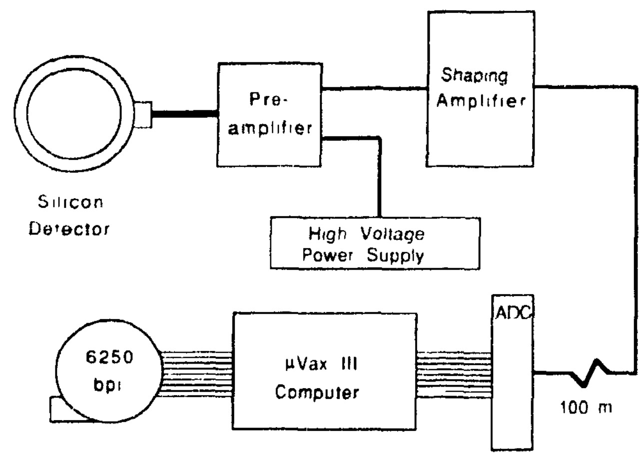

Figure 2.3 Silicon detector electronics

charge integration over a finite time window is equivalent to a measure of the pulse height. A synchronized gate of 180 ns width was used to sample the maximum of the peak The data from the ADC, along with the other data from the E814 detectors, are written by a μVax III to 6250 bpi tapes. Events are recorded a rate of 40 events per beam spill.

Particles that are minimum ionizing have a small energy loss of the order of ~ 150 keV in the silicon detector Therefore, reduction of the noise level is important. The first source of noise was eliminated simply by protecting the detector from light. A short microdot cable (~ 20 cm) was used between the detector and the preamplifier in order to reduce the capacitance of the connection. The detector holder, made of aluminium, acted as an antenna and through a capacitive coupling was initially inducing strong 60 Hz fluctuations. Part of the holder was replaced by teflon to improve the isolation of the silicon detector and thereby removing the effect of the ground loop After this modification, no 60 Hz contribution could be seen at the shaping amplifier level Finally, the position of the minimum ionizing particle peak is used for calibration and the electronic noise is estimated from the pedestal width as discussed in section 3.2.

The 992 NaI TCAL crystals are individually read by Phillips AV29 vacuum photodiodes The signals are fed through low-capacitance short cable (< 5 cm) to low-noise, charge-sensitive integrating preamplifiers. The output of the preamplifiers are sent through 75 m cables to shaping amplifiers. The outputs of the shaping amplifiers are split into two parts. One third of the signal's amplitude is sent to LeCroy 1882 FASTBUS charge integrating ADC's for digitization A gate of 200 ns width centered around the negative peak of the bipolar pulse is used to sample the collected charge The remaining two thirds of the signal amplitudes are used by the trigger system The analog signals of each adjacent two rows of crystal are summed Resistors are used to produce weighted sums in order to simulate the $\sin\theta_i$ dependence of the individual crystal contributions to E_t The weighted sums are digitized with LeCroy 4300B FERA ADCs This procedure is accurate to within ±10% of the measured $\sin\theta_i$ values and provides a fast signal proportional to E_t The effect of the electronic noise in individual ADC channels on the pedestal width averages to 1.48±0 42 MeV A more detailed discussion of the TCAL electronics and its use in the trigger system of the E814 experiment is found in [WA90].

2.4 Trigger System

The E814 experiment has a wide research program, as outlined in section 2.1, for which a flexible data acquisition system trigger was developed. The main data and decision flow of the elaborate E814 trigger are schematically shown on figure 2 4 [TA91]

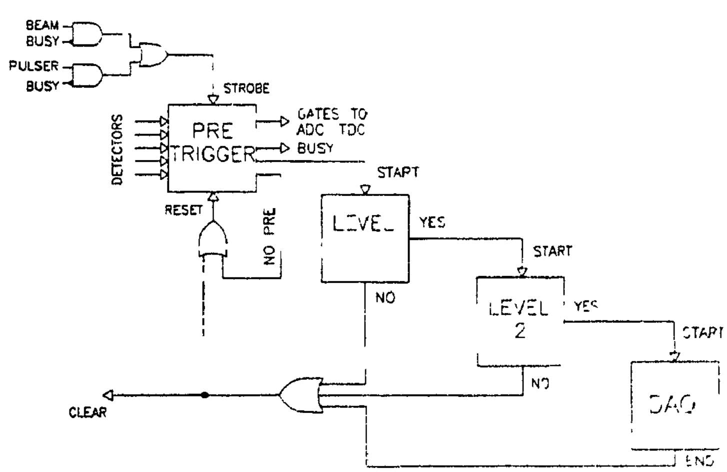

Figure 2.4 Schematic representation of the E814 trigger system.

The first level of decision is the pretrigger. It supplies the gates for the ADC's and TDC's (Time-to-Digital Converter) of the experiment and starts the first level of the trigger logic. A typical pretrigger for central collision studies is an interaction trigger which requires a valid beam particle, a minimum number of target scintillators firing and a minimum multiplicity. Once the pretrigger gives a start, the level 1 and level 2 triggers are activated. Examples of the conditions tested at these levels are: various levels of charged particle multiplicity, transverse energy in the PCAL or the TCAL, time of flight in the forward spectrometer, charge of the particles in the forward spectrometer. The different selections of reaction conditions provide triggers such as the beam trigger, which is a minimum bias trigger only requiring a good beam particle, or the centrality trigger requiring a minimum transverse energy.

The data taken for the present work was acquired in parallel with the anti-matter production measurement of the E814 program. This study used a late timing trigger which requires particles in the FSCI's of the forward spectrometer that are delayed relative to the beam velocity particles. The time of flight gate was selecting events with particles coming 4 ns after particles with the speed of light. The event characterization of this trigger is discussed in more detail in section 4.3. A complete description of the trigger is given in reference [GR91].

2.5 Counting Rate Estimate

The silicon detector has a finite surface which implies that two particles may hit it at the same time. To reduce this effect, the covered solid angle has to be minimized. On the other hand, the need for statistics calls for a maximization of the counting rate. As an approximation, if the probability of having n particles through the detector is assumed to be given by a Poisson distribution (uncorrelated particles)

$$P(n;\mu) = \frac{e^{-\mu}\mu^n}{n!}, \tag{2.1}$$

then the ratio of double to single hits is given by:

$$\frac{P(2;\mu)}{P(1;\mu)} = \frac{\mu}{2}, \tag{2.2}$$

where μ is the mean number of particles that hit the detector per event. The counting rate is proportional to the number of particles emitted per unit of solid angle per reaction. The mean number of particles is not well known but a theoretical model like HIJET (described in section 4 1) can be used to estimate the yield of particles in different angular ranges The experiment E802 covers θ angles up to 150° in the laboratory frame and measurements of the charged particle yield are in good agreement with the theoretical predictions of HIJET Therefore, this model is used to estimate the yield of charged particles According to HIJET, the yield goes from ~ 10 particles per steradian per event at 55° to ~ 2 part/sr/event at 135°

In section 1.3, it is predicted that reasonable particle identification can be achieved around 70°. With formula 2 2 one calculates that a reasonable proportion of double hits ($\sim 5\%$) is obtained by limiting the counting rate of the silicon detector to 0 1 particle per event. If one assumes a yield at 70° of ~ 10 part/sr/event, to limit the counting rate at 0 1 part/event, implies that the detector has to cover a solid angle of $\Omega \approx 0.01$ sr Therefore, a silicon detector with a surface of 300 mm^2 must be placed at ~ 17 cm from the target (taking into account its orientation). The typical solid angle covered by a crystal of the target calorimeter (TCAL) around 70° is $\Omega \approx 0.015$ sr, which is of the same order as the solid angle covered by the silicon detector Finally, one can estimate the total number of events Each tape contains ~ 5000 events, assuming a counting rate of ~ 0.1 part/event, for 50 tapes, one expects to record a total of 25000 hits in the silicon detector.

3

Measurements

3.1 Available data

The silicon detector test was scheduled during a five-day anti-matter study in June 1990. The beam particles, ^{28}Si, were accelerated by the AGS at a momentum of 14.6 GeV/c per nucleon. The beam intensity was limited to a rate of $\sim 10^5$ particles per second. Three targets were used for the part of the run where the test was conducted. They were: 2.64 g/cm^2 Al, 5.72 g/cm^2 Cu and 11.33 g/cm^2 Pb. During this period, fifty-eight 6250 bpi tapes of ^{28}Si + Pb data were written, fifty-two with a Cu target and fifty-three with the Al target.

Each tape contains roughly 5000 events of which a small fraction have a particle going through the silicon detector (silicon events). In the case of the Pb target, for example, only $\sim 3\%$ of the recorded events have a signal above pedestal in the silicon detector. This fraction is lower than predicted in the first simulation of section 1.3, mainly because the experimental trigger (late timing trigger) is more peripheral than assumed in the calculations (see section 4.3). Because of the larger center of mass rapidity, the fraction of silicon events goes down to $\sim 1.5\%$ and $\sim 1\%$ for the copper and aluminium targets, respectively. For the silicon events, $\sim 20\%$ also have a signal above the pedestal in the corresponding crystals of the TCAL. This implies that only 0.6% of the all recorded events of the Pb target can be used to make correlations between the signal of the silicon detector and the signal of the TCAL crystals. Because of the low statistics accumulated for these two light targets (Al and Cu), the present analysis concerns only the lead target data.

3.2 Calibration of the Silicon Detector

Because of the long cables between the silicon detector and the counting house the electronics are prone to 60 Hz noise. Thus, the signal from the silicon detector is first checked for 60 Hz noise which would worsen the resolution The raw signal from the silicon detector is plotted as a function of the 60 Hz phase in figure 3 1 This spectra was accumulated over 15 lead target runs to increase the statistics (individual runs are similar). The horizontal band ($\leq$ 200 ADC channels) is the pedestal Since no 60 Hz phase dependent structure of the pedestal is observed, one concludes that it is not a significant component of the electronic noise

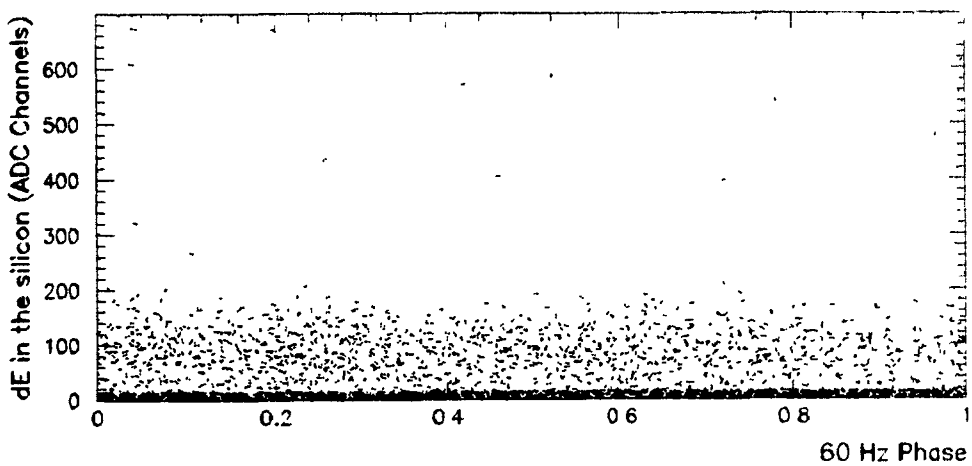

Figure 3.1 Correlation of the signal of silicon detector vs the 60 Hz phase

Minimum ionizing particles leave the same energy in a dE detector independent of their total energy. Therefore, the signals from all the MIP's accumulate to form a minimum ionizing peak in a dE spectra. A typical spectrum obtained for the lead target is shown in figure 3.2. The spectra was accumulated over 15 runs and is plotted on a logarithmic scale so that all the features are visible. The tall peak near channel 90 is due to the pedestal of the ADC. It corresponds to events where the data acquisition was triggered but no particle went through the silicon detector. The first bin on the left corresponds to the negative part of the pedestal and the last one on the right, to overflows of the ADC The peak near channel 500 corresponds to the most probable energy loss of MIP's as measured in ADC channels by the silicon detector.

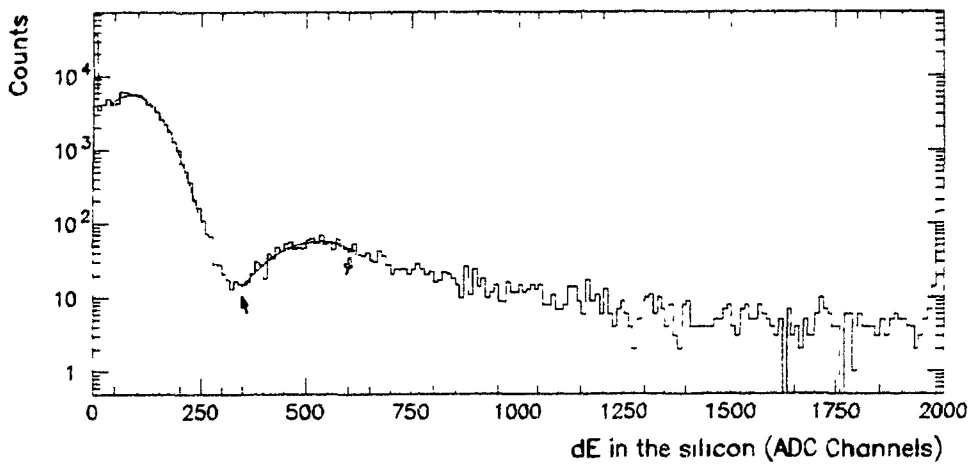

Figure 3.2 Raw signal from the silicon detector Gaussian fits are made on the pedestal and the minimum ionizing peak

The position of the pedestal has been determined by a gaussian fit shown by a solid line on the left of figure 3.2. The mean of the pedestal is at channel 80 with a standard deviation of $\sigma \approx 61$ channels. The most probable energy loss was obtained with a second gaussian fit from the left side of the MIP peak to slightly past the maximum of the peak to evaluate the most probable energy loss value (indicated with arrows in figure 3.2). The fit gives a most probable energy loss value of 520 ADC channels. The value of 180 keV given by GEANT for the most probable energy loss is used to calibrate the silicon detector. Setting the value of the most probable energy loss at 180 keV and the mean of the pedestal at 0 keV gives a calibrated standard deviation of $\sigma \approx 24$ keV which is consistent with the measurement of the electronic noise presented in section 2.3.2. The value of 180 keV for the most probable energy loss given by GEANT is somewhat different from the value calculated using reference [HE90] i.e. 141 keV.

3.3 Analysis Routines for the TCAL

When a high energy particle hits a calorimeter, a shower develops with a finite lateral extension. A single particle can leave its energy in up to 9 adjacent TCAL crystals thereby forming a cluster. The proper energy and number of particles is obtained by using a clustering routine [DA91].

The raw data are analyzed in the following way The signals given by each crystal are first calibrated with the help of cosmic ray data taken before and after the beam time [WA90]. The pedestals are subtracted. A cluster-finding routine divides the crystals into two groups: centers and neighbors To be considered as a center, more than 30 MeV must have been deposited in a given crystal and it must be a local maximum A local maximum means that no larger energy deposition is observed in adjacent crystals Neighbors are next to a maximum and have a signal of at least 5 MeV The energy of a cluster is then given by the sum of the energy of its center and of all its neighbors If two centers are separated by only one crystal, the energy of the common neighbor is shared according to the ratio of the energies of the centers The energy measured by crystals that are not part of any cluster is set to zero. The cluster energies are then used to compute information such as the total energy, hit multiplicity and transverse energy [DA91].

When a hit is found in the silicon detector, the three crystals behind it are searched for the presence of a cluster. If a cluster is present, its energy is assumed to come from the same particle that went through the silicon detector. When the cluster finding routine is used in coincidence with hits in the silicon detector, one reduces the effects of leakage of energy in the neighboring crystals. This also prevents the overestimation of the energy of a particle when common neighbors are present.

3.4 Relative Position Determination

To understand the response of the Si-TCAL telescope it is important to know exactly the relative positions of the silicon detector and the TCAL crystals. This is done by making a correlation of the hits in the silicon detector and in the TCAL crystals. Individual crystals are labelled by a set of two numbers (ϕ,θ). The first number corresponds to the azimuthal angle ϕ (from 1 to 64) as shown in the front view of the target region presented in figure 3.3. The second number corresponds to the polar angle θ (from 1 to 20) as shown in the side view of the target region presented in figure 3.3

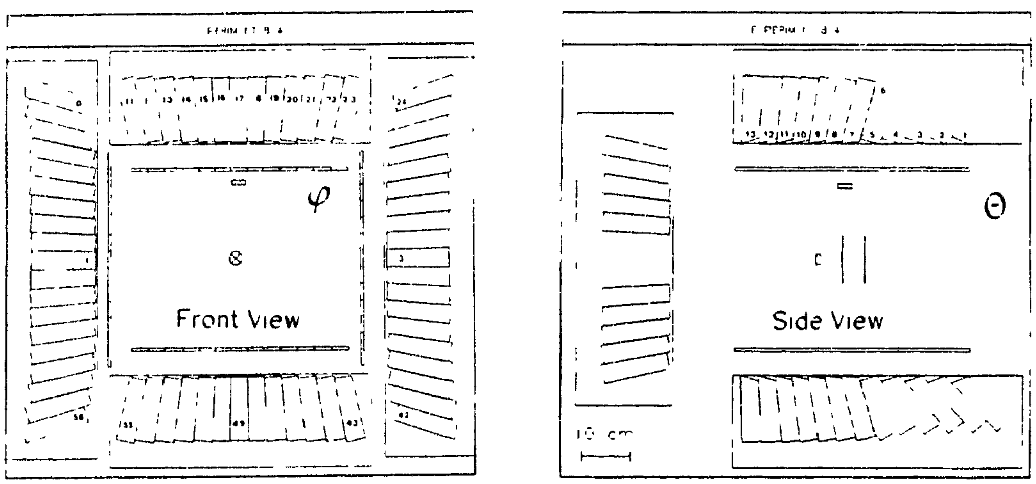

Figure 3.3 Numbering scheme of the TCAL crystals. The beam direction is shown at the center of the front view.

A first evaluation of the position of the silicon detector relative to the TCAL crystals can be made from figure 3.4. The axis correspond to the ϕ and θ numbers assigned to each crystal. Therefore, each bin of figure 3.4 corresponds to a crystal of the TCAL. The bins are incremented when a cluster at the corresponding TCAL crystal is found to be in coincidence with a signal in the silicon detector. As expected, the background is larger for the most forward polar angles (small θ). The tallest peak is observed for crystal (17,5) indicating that the silicon detector is best aligned with this crystal. The excess hits in crystals (17,6) and (17,7) imply that the the silicon detector solid angle also covers these crystals. One can see in figure 3.3 that the geometry

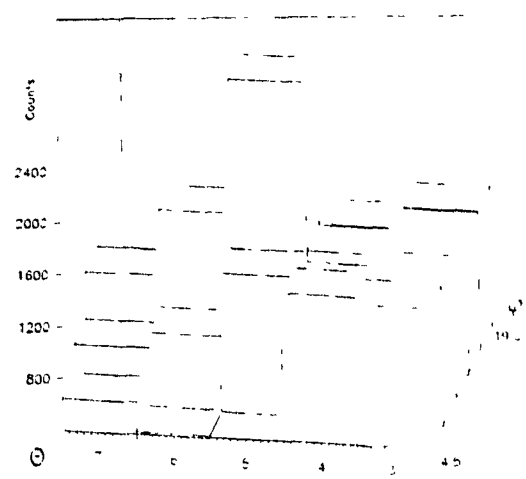

Figure 3.4 Number of hits per crystal in coincidence with the silicon detector (accumulated over 58 lead target runs).

of these three crystals is not perfectly projective Therefore, a particle that hits the silicon detector can sometime traverse more than one crystal.

The following method is used to determine the angular position of the silicon detector with better accuracy. Out of the three crystals behind the silicon detector (17,5), (17,6) or (17,7), the events where only the crystal (17,5) or (17,7) are hit are analyzed ((17,6)'s solid angle is different). The relative rates of coincidence with the silicon detector are related to the angular alignment of the corresponding TCAL crystal with the silicon detector. Therefore, the ratio of the number of single coincidences in crystal (17,5) and in crystal (17,7) is a measure of the alignment of each crystal relative to the silicon detector. The position of the silicon detector is determined by reproducing this ratio through simulations.

The single coincidence ratios were calculated, using the particle generator described in section 4.2, for five positions of the silicon detector as shown in figure 3 5 The positions, θ of the silicon detector are given relative to the positions of the TCAL crystals. The single coincidence ratio is largest when the silicon detector is facing the crystal (17,5) at 75° and is the smallest when facing (17,6) at 68° The value of this ratio from the data is $(17,5)/(17,7) = 0.7$. By interpolation, the actual angular position of the silicon detector is deduced to be $\theta = 70 \pm 1°$. This is considered to be precise enough for the purpose of the test since the angular segmentation of the TCAL

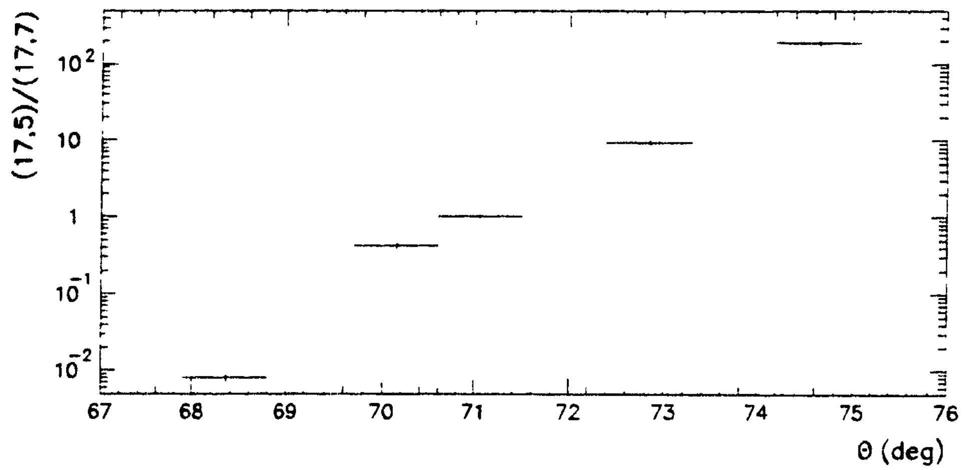

Figure 3.5 Relative position determination.

is of the order of $\Delta\theta \sim 4°$.

3.5 Double Hit Rate Evaluation

In section 2.5, the probability for two particles to hit the silicon detector at the same time was estimated to be of the order of 5% on the basis of the theoretical model HIJET. Out of 432000 events on 53 Pb tapes only 12800 have a signal above pedestal in the silicon detector. This makes an average of 0.03 hits per event in the silicon detector. This lower value than obtained in section 2.4 is attributed to the more peripheral experimental trigger (discussed in section 4.3) than assumed in the calculation. Assuming that the probability of double hits can be represented by a Poisson distribution as in formula (2.1) and with a mean occupancy of 0.03 hits per event, the proportion of double hits according to formula (2.2) is then 1.5%. Such a low double hit rate from uncorrelated particles is considered to form a insignificant background. However, this background could be more important for correlated particles like e^+ and e^- from the two-γ decay of the π°.

The probability of double hits in the TCAL crystals is obtained by comparing the counting rates of the crystals behind the silicon detector with those positioned symmetrically in the opposite wall of the TCAL. Figure 3.6 shows a slice of the TCAL presenting the crystals with polar number $\theta = 5$. The number of clusters found in

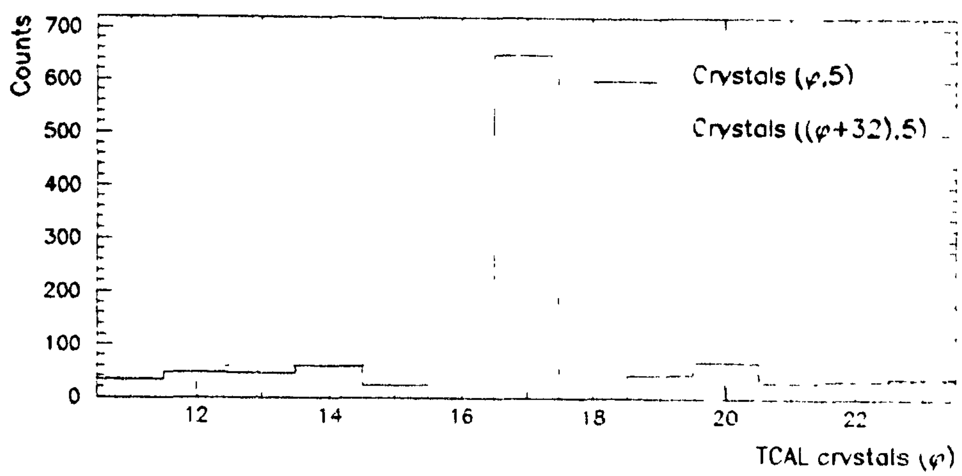

Figure 3.6 Double hits in the TCAL crystals. The solid line is for the crystals from (11,5) to (23,5) and the dotted line from (43,5) to (55,5)

coincidence with a hit in the silicon detector and a cluster in (17,5) are plotted for each crystal between (11,5) and (23,5) (solid line) and for each crystal between (43,5) and (55,5) (dashed line). The histogram was accumulated over 15 runs The dotted line is plotted so that the symmetrical crystals relative to the beam axis are overlaid (the symmetrical crystal to (17,5) is (49,5)) As expected, a peak is seen at the position of the silicon detector at crystal (17,5) The number of clusters found in (16,5) and (18,5) is zero since a cluster is required in (17,5) An evaluation of the proportion of double hits in the TCAL crystals is obtained from the ratio of the probabilities of having a hit in these two crystals in coincidence with the silicon detector The observed ratio is 17%. The double hit proportion in TCAL crystals is large since it is sensitive to charged particles as well as neutral particles and gamma rays. The requirement of a hit in the silicon detector also favors more central events having higher multiplicity.

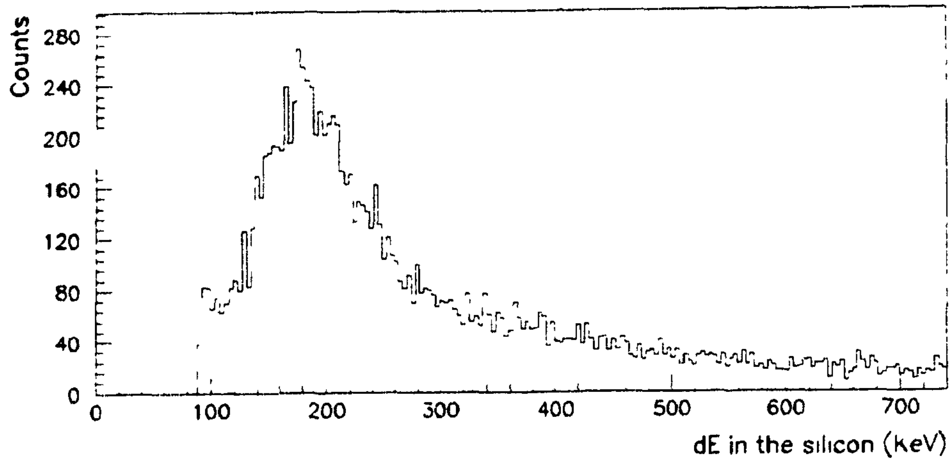

Figure 3.7 dE in the silicon detector.

3.6 Results

The data presented in this section were accumulated over 58 runs with the lead target for a total of 465800 events The energy loss spectrum in the silicon detector is shown in figure 3.7. The pedestal is suppressed so that the interesting features are visible The spectrum is characterized by the presence of a minimum ionizing peak at 180 keV followed by a long high energy tail. One notes that the general shape of the measured spectra is well described by the calculated energy loss spectra predicted by the initial simulation (showed in subsection 1.3.1).

Figure 3.8(a) shows a scatter plot of the pulse height in the silicon detector vs the cluster energy in the TCAL crystals behind the Si. When a signal above pedestal is detected ($dE > 100$ keV) in the silicon detector, the three TCAL crystals behind the silicon detector ((17,5),(17,6),(17,7)) are searched for the presence of a cluster. If a cluster is found, the corresponding histogram bin is incremented. The pedestal region of the silicon detector pulse height is not plotted in order to enhance the interesting parts of the graph. Figure 3.8(b) and 3.8(c) show projections onto the Y and X axes, respectively. The MIF peak of figure 3.8(b) is more pronounced than in figure 3.7. The shape of the energy loss spectra is different because of the requirement of a cluster in the TCAL crystals which favors the most energetic particles. A peak with a high energy tail is present at about 0.6 GeV in the TCAL cluster energy spectrum of figure

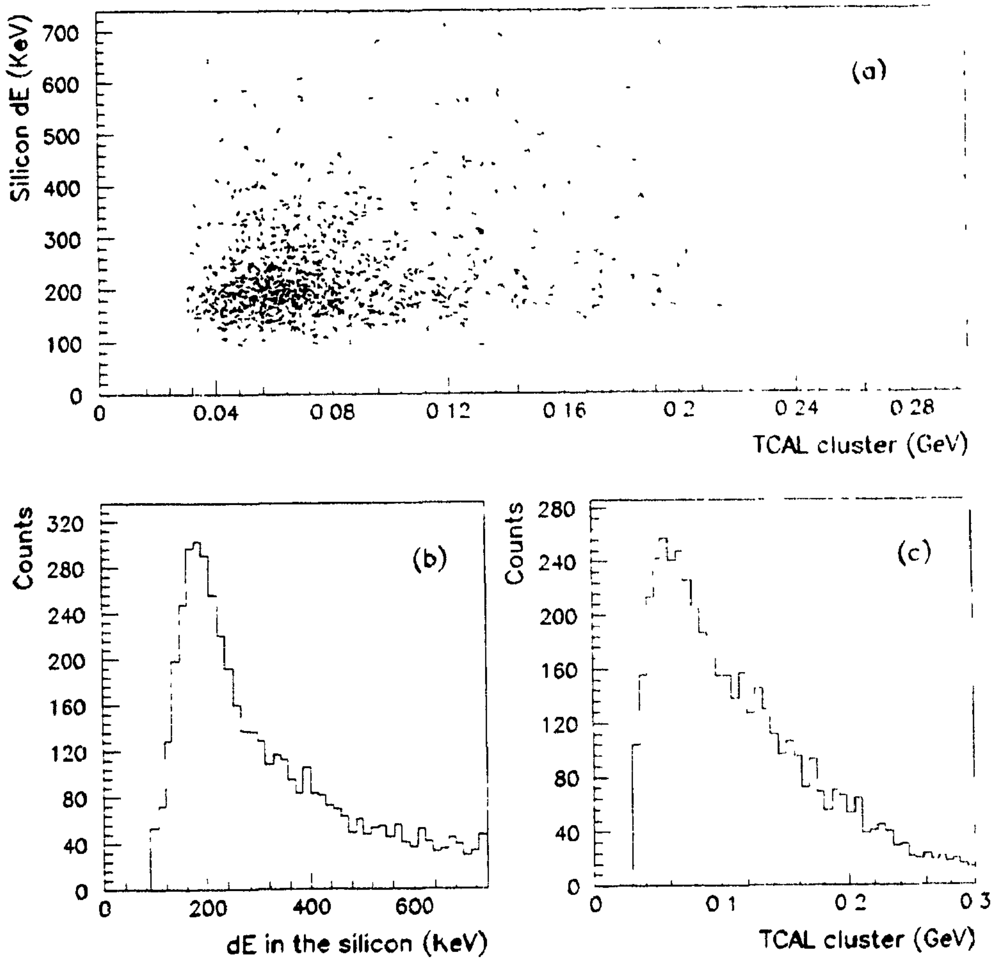

Figure 3.8 dE vs E telescope detector. (a) dE in the silicon detector vs E measured by the cluster routine. (b) dE in the silicon detector (projection on the y axis). (c) E in the TCAL (projection on the x axis).

3.8(c). The feasibility of particle identification using the silicon detector alone and using the telescope ensemble is analysed in the next chapter on the basis of computer simulations.

4

Discussions

The first section of this chapter describes the event generator and the tracking program used for all the simulations presented in this work. It is followed by a description of the three rounds of simulation which were carried out. In order to compare the response of each detector for different types of particles, the detector responses were first simulated using a single particle generator Tracking of complete HIJET events was used to understand the trigger bias via its influence on the transverse energy spectra. The trigger bias was then included in a more complete simulation during which nearly all the backgrounds were included.

4.1 The HIJET and GEANT programs

The detailed response of the silicon detector and TCAL combination is simulated with the event generator HIJET and the tracking program GEANT. HIJET is an event generator code developed at BNL in the early 80's to model high-energy heavy-ion collisions [LU85]. In this model, the dynamics of the nucleus-nucleus collisions are taken as a superposition of independent hadron-hadron collisions. Each nucleon is given a Fermi momentum according to a Gaussian distribution. The interactions between nucleons are simulated using the Monte Carlo code called ISAJET [PA82] Nucleons that have interacted acquire a new four-momentum but, for simplicity, maintain their original positions From the produced particles, HIJET selects the forward and backward leading baryons and allows them to re-interact The other particles (secondaries) materialize along the center of mass trajectory of the parent particles. When a secondary interaction occurs, the produced particles may interact (rescatter) depending on their formation time.

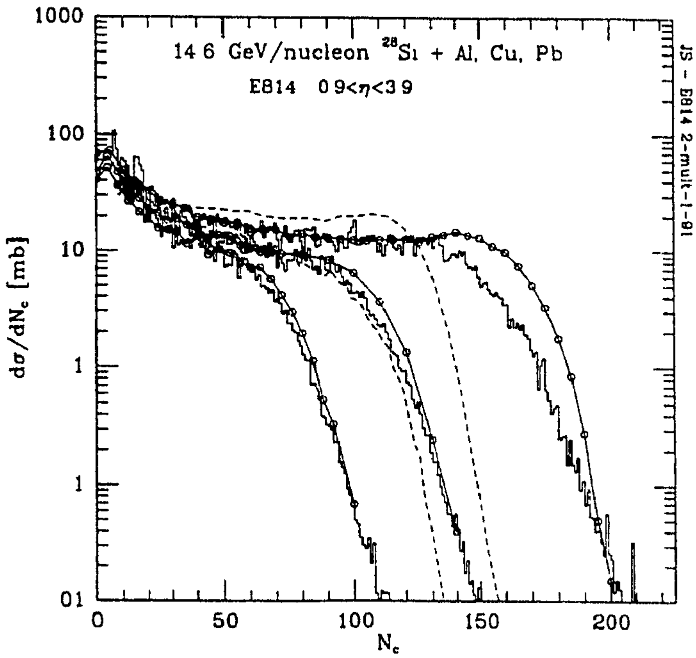

Figure 4.1 Measured multiplicity distributions compared to the predictions of HIJET.

HIJET reproduces well such global variables as average multiplicities and rapidity distributions at AGS energies provided that secondary interactions are included [SH89] This is shown in figure 4.1 where is presented the charged particle multiplicity as measured by E814 multiplicity detector, for three targets (Al,Cu,Pb) [BA91B]. The curves with circles are generated using HIJET with rescattering and the dashed curves are without rescattering. Excellent agreement between HIJET and experimental data is observed when rescattering is included while HIJET without rescattering predicts far fewer particles than experimentally observed for the lead target A more detailed presentation of the results of HIJET and a comparison with the prediction of other event generator at the present energy is found in [WA90]

The HIJET simulations presented in this chapter all included the following features: secondary interactions, ρ and Δ decays and spectator nucleons. The energy in the nucleon-nucleon center of mass was set at 5.41 GeV. The impact parameter of the collisions was uniformly distributed in the interval 0 fm < b < 10.8 fm (centrality 1.0).

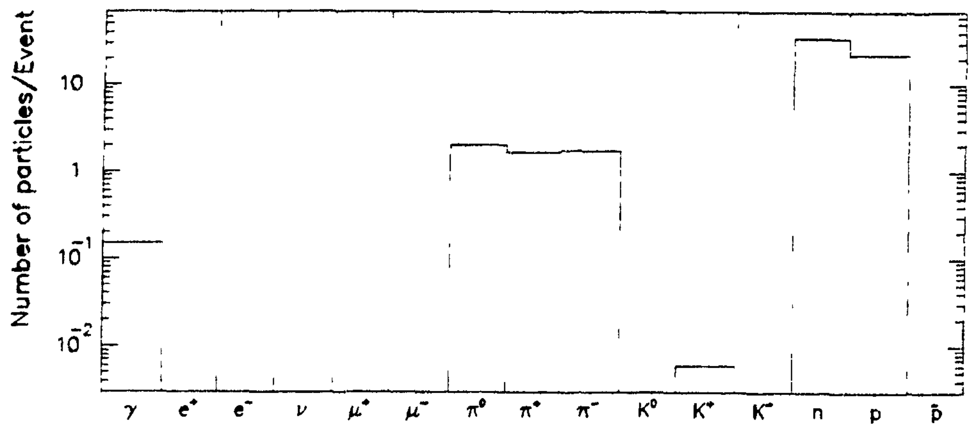

Figure 4.2 Particle inventory from HIJET in the range $60° < \theta_i < 80°$

An inventory of the types of particles produced by HIJET for 500 Si + Pb events with the parameters described above is presented in figure 4.2. The inventory is limited to the angular domain of $60° < \theta_i < 80°$ since the test detector is positioned at $\theta = 70°$. The silicon detector is only sensitive to charged particles. Therefore, this figure indicates that, according to this model, only initial protons and pions will contribute significantly to measured spectra.

The particles generated by HIJET have to be tracked through the detector system. This is done with the program GEANT [BR87] which is commonly used to model high energy experiments and to simulate the propagation of high energy particles through matter. Particles with given initial energy and momentum are tracked through each component of the modeled setup detectors and passive material. This tracking can be done with various degrees of sophistication provided that sufficient computer time is available. After the tracking of an event is completed by GEANT, the same algorithms and cluster routines that are used in the data analysis are used to generate the calculated spectra.

For the simulation presented in this chapter, a realistic configuration of the experimental setup (as shown in figure 3.3) is included in GEANT. All detectors shown in this figure are included in the detailed simulations except the Si Multiplicity detector. This configuration includes, in particular, all the crystals that make up the target calorimeter, with their shapes and positions. The TPADs are simulated as dead material. The silicon detector is modeled with its proper dimensions and orientation.

The program GEANT simulates the interaction of particles with matter with different levels of sophistication. Physical processes can be included in the calculation separately in order to study their effects on the measurements. In all the simulations described in this chapter, the following processes are included in the calculations. Positrons are allowed to annihilate leading to the production of γ rays. Pair production and photoelectric emission by γ are also included. Secondaries are produced during the stopping processes of the particles and are tracked. The energy loss fluctuations are generated according to Landau distributions. The multiple scattering probability is modeled with a Gaussian distribution. Delta ray production, Bremsstrahlung and Compton processes are also included.

4.2 Detector response study with single particles

The response of the detector system to each type of particles involved in the reactions is first studied by tracking single particles of given types. This procedure corresponds to the initial simulation described in section 1.3, but with the TCAL and the silicon detector modeled more exactly.

A Monte Carlo single particle generator program was developed to study the response of the detectors to each type of particles. It also improves the calculation efficiency by reducing the number of HIJET events that have to be generated and scanned. In this program, the particles are generated according to the momentum distributions obtained from HIJET. The initial momentum spectra for p and π^+ as produced by HIJET are shown in figure 4.3 (π°, π^- and π^+ all have similar distributions). This histogram is obtained from an inventory of the particles with initial direction $60^\circ < \theta_i < 80^\circ$ of 500 Si + Pb events. The spectra for pions are essentially thermal

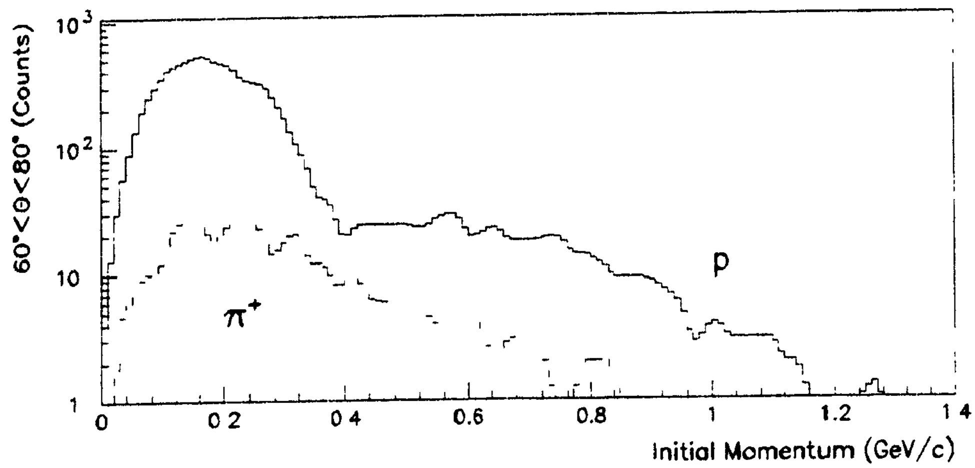

Figure 4.3 Initial momentum spectra for p's and π's. HIJET predictions for the interval $60^\circ < \theta_l < 80^\circ$. The distributions are smoothed to suppress the high frequency statistical variations.

and decrease exponentially with momentum. The proton spectrum is understood as a sum of a spectator peak centered at ~ 150 MeV/c and a thermal spectra spectrum which forms the high momentum tail and decreases exponentially with momentum. The single particle generator produces particles statistically distributed according to the momentum spectra shown in figure 4.3. It uniformly fills a cone of $\Omega = 0.01$ sr in the direction of the silicon detector. This program allows a rapid determination of the expected response of the detectors to each type of particles.

For this round of simulations, 10 000 protons and proportional numbers of pions were generated using the particle inventory of figure 4.2. As the description used for the TCAL is more sophisticated, the results should be closer to what can be expected from the detector system. The spectra of energy loss in the silicon detector are plotted in figure 4.4 for four types of particles. The same features as in the initial simulations are present (see subsection 1.3.1). The protons, because of their low energies and thus, higher energy loss rates, peak at 300 keV and are spread on the right of the energy loss spectra. The charged pions are largely concentrated in the minimum ionizing peak at ≈ 180 keV. The neutral pions all decay within the target ($\tau = 8.4 \times 10^{-17}$ s) into two γ rays. The γ rays can undergo Compton scattering, photo electric effect or annihilate through pair production and produce electrons and positrons. The charged e^- and e^+ would leave a signal in the silicon detector. However, since the two γ's

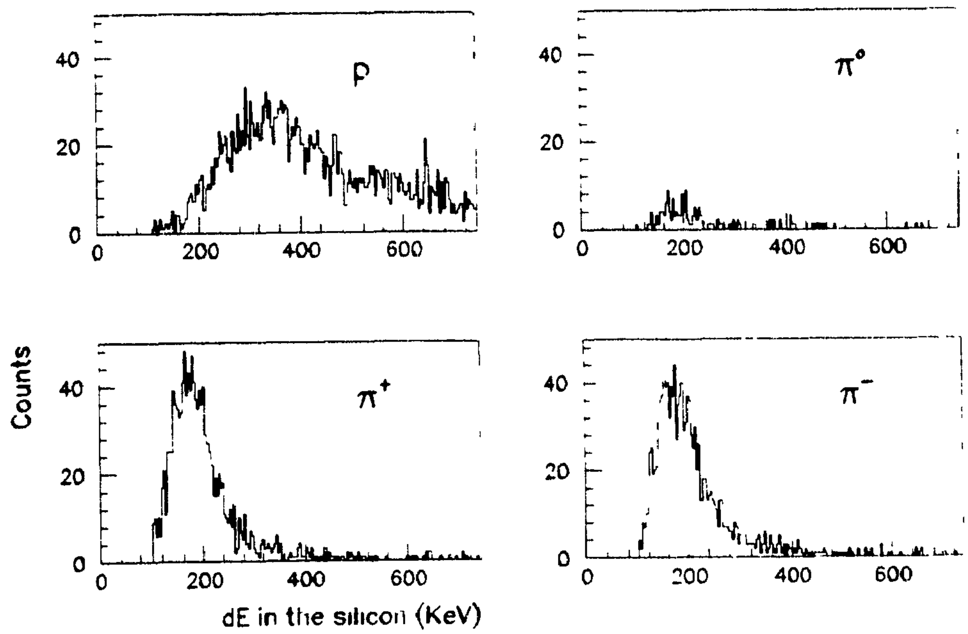

Figure 4.4 dE for p, π°, π^+ and π^- from the single particle event generator

are emitted in opposite direction in the center of mass of the π°, the subsequent e^- and e^+ are not produced in the initial direction of the π° Moreover, the e^- and e^+ have small masses and are therefore easily deviated from their trajectories Since, in the present simulation, the π° are generated within a small cone centered on the direction of the silicon detector, this implies a net loss in the number of e^- and e^+ at the silicon detector This explains the low number of entries in the labelled π° spectra Nevertheless, because of their low mass, most of the e^- and e^+ that hit the silicon detector are minimum ionizing.

The experimentally measured spectra corresponds to the sum of the contributions from each type of particle. The normalization of the simulated histogram was adjusted to the best description of the experimental data. The summed spectra are presented in figure 4.5 (solid line). The calculation reproduces well the shape of the experimental spectrum (dotted line).

The correlations between the calculated energy loss in the silicon detector and the calculated energy loss in the TCAL crystals for four types of particles are shown in

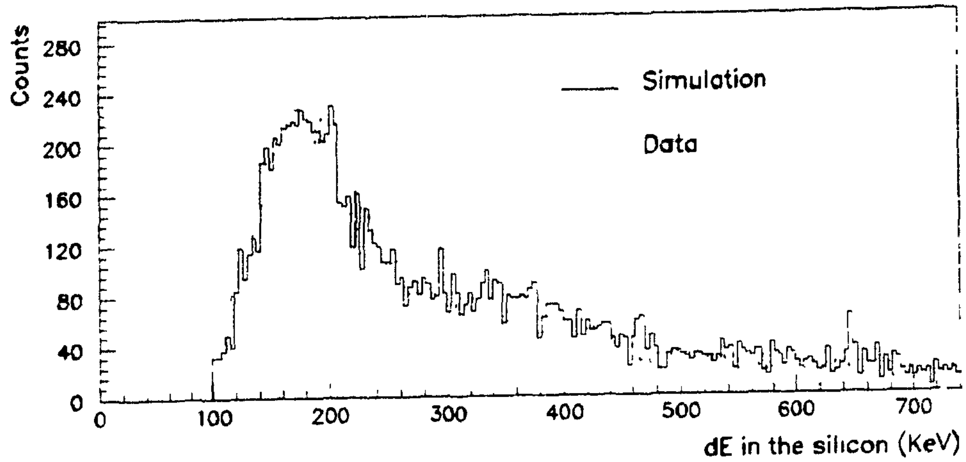

Figure 4.5 Total dE from single particle generator.

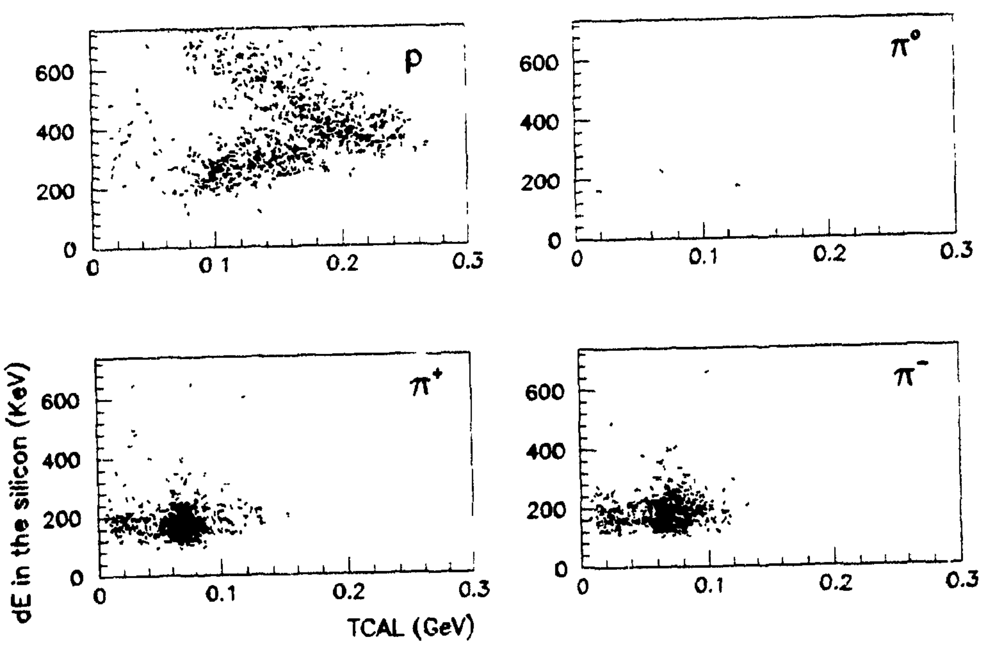

Figure 4.6 dE vs E for p, π°, π^{+} and π^{-} as given by the single particle generator.

figure 4.6. One observes that most of the charged pions are predicted to be minimum ionizing in both detectors and are grouped in the lower left part of the graph. The e^{-} and e^{+} produced from the decay of neutral pions are also minimum ionizing in the silicon detector because of their small masses but they leave a broad range of signals in the TCAL. In agreement with the initial simulation (described in section 1.3), protons

form a band which bends when they are sufficiently energetic and punch through the calorimeter at E > 0.2 GeV. However, the distributions are much wider than obtained in the initial simulation. This can be attributed to the more detailed description of the non-uniform geometry of the TCAL Leakage between the crystals and imperfect reconstruction of the particle energy by the cluster routine also increase the widths of the distributions.

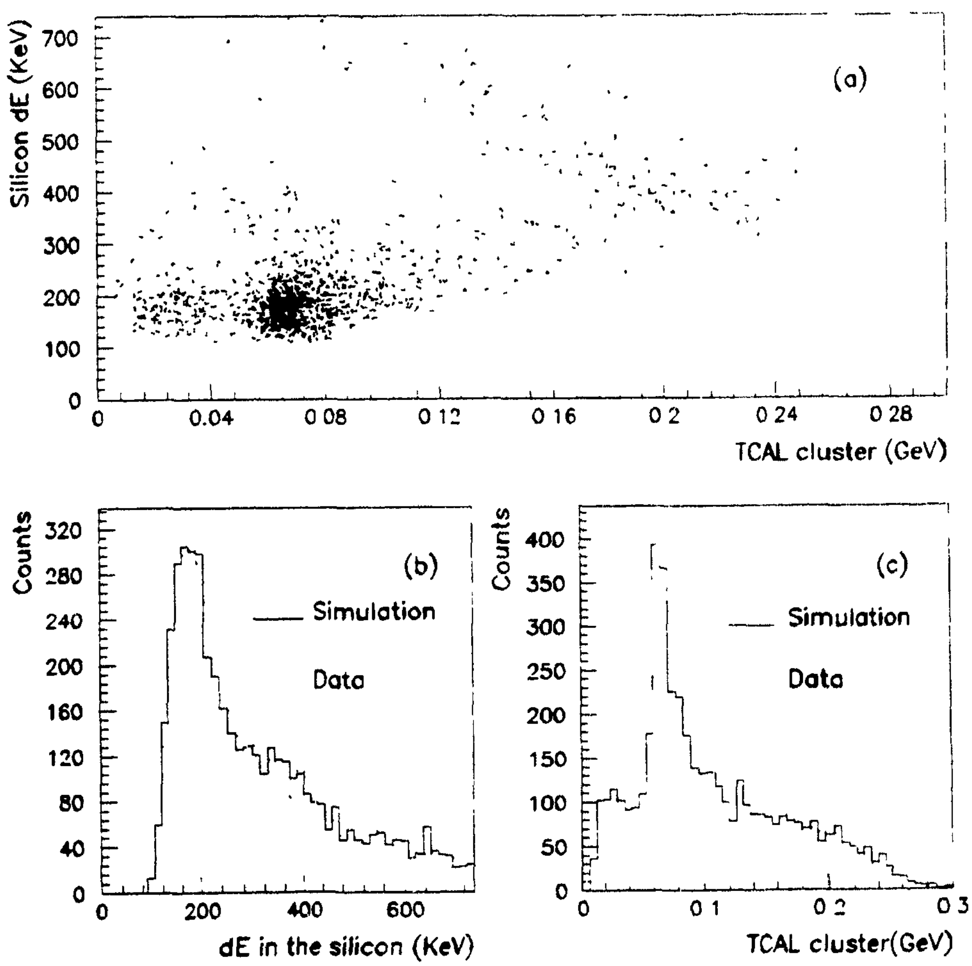

Figure 4.7 Total dE vs E from the single particle generator (a) dE vs E matrix. (b) dE in the silicon detector. (c) Cluster energy measured in the TCAL.

The summation of each contribution is shown in figure 4.7(a). Although the particles are not as localized as in the initial simulation, structures are still clearly visible. This contrasts with the data shown in figure 3.9 which are structureless

The projections on each axis of the dE vs E matrix are shown in figure 4.7(b) and 4.7(c). The two projections are scaled to the data to allow an easier comparison. Figure 4.7(b) corresponds to the energy loss spectra in the silicon detector for the particles that also leave a signal in the TCAL (solid line). A minimum ionizing peak is visible at 180 keV and a high energy loss rate tail is also present. The MIP peak of figure 4.7(b) is more pronounced than in figure 4.5 since the requirement of a corresponding cluster in the TCAL favors the most energetic particles. The shape of this spectra is consistent with the experimental data as is shown by the dotted line. The calculated cluster energy spectra shown in figure 4.7(c) (solid line) features a narrow peak at 0.075 GeV due to minimum ionizing particles. However, such a peak is not present in the experimental data (dotted line). This peak results from the π which are grouped in the minimum ionizing part of the dE vs E matrix.

In summary, this simulation using the proper geometry fails to reproduce the observed particle distributions. The prediction of an unobserved peak in the TCAL spectrum, the structure present in the dE vs E histogram and the net loss of e^- and e^+ all indicate the need for a more complete simulation; in particular, one that would treat total events.

4.3 Trigger bias correction

To provide a more realistic simulation, it is important to include the proper distribution of impact parameter resulting from the experimental trigger. The late timing trigger used in the present test (see section 2.4) requires events with particles that arrive in the downstream FSCI 4 ns after prompt particles. The distribution of impact parameter is thereby modified compared to a minimum bias trigger. Thus, the trigger bias introduced by the experimental trigger has to be understood. Only then can the tracking of events properly simulate some of the backgrounds such as double hits.

It is known that the charged particle multiplicity is an observable which is well correlated with the centrality of the event since central events produce more particles than peripheral events [TI88]. The yield of charged particles as function of pseudo-

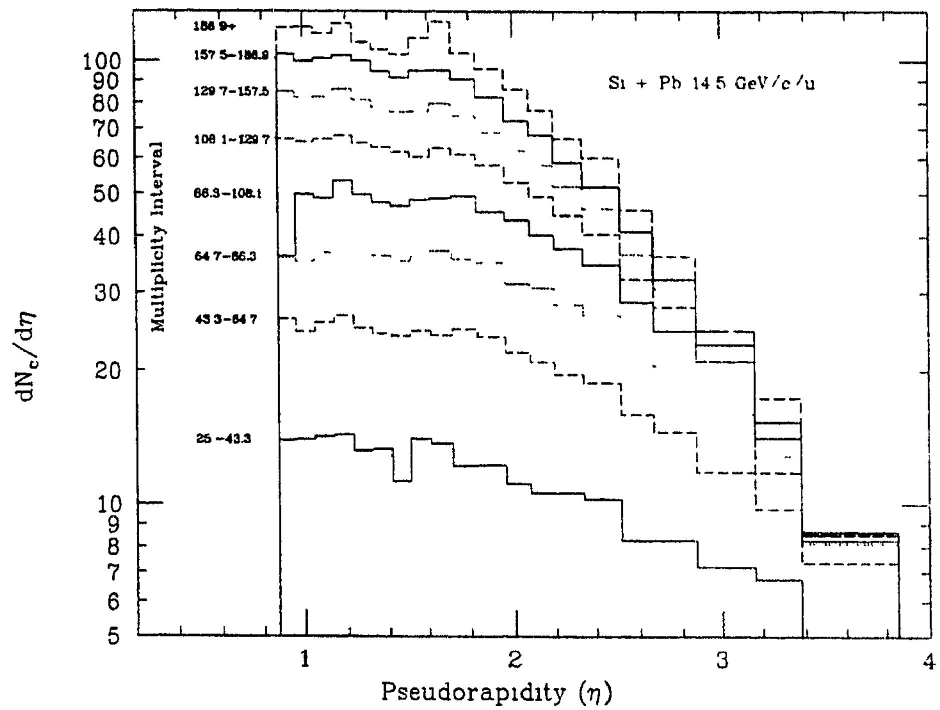

Figure 4.8 Multiplicity distributions. $dN_c/d\eta$ for various multiplicity cuts as measured by E814.

rapidity for various total multiplicity intervals as measured by the E814 multiplicity detector is shown in figure 4.8 [BA91B]. One observes that the yield of particles in a given angular range is a strong function of the total multiplicity and thus, of centrality. This confirms that, in order to understand the response of the detectors, the proper impact parameter distribution has to be included in the simulations.

Like the multiplicity, transverse energy is a global observable which is strongly correlated with the centrality of the event [TI88]. In the present analysis, the transverse energy as measured by the TCAL is used to study the effects of the trigger bias. Figure 4.9 shows the experimental TCAL E_t spectrum obtained with the late timing trigger as compared to the E_t spectrum corresponding to a minimum bias trigger. This last spectrum is obtained using the beam trigger (outlined in section 2.4) The transverse energy is computed from the energy obtained using the TCAL cluster routine One notes that the late timing trigger has a tendency to enhanced events with low E_t (peripheral interactions) at the expense of high E_t events (central collisions) This effect is due to the acceptance of the forward spectrometer and is discussed in reference

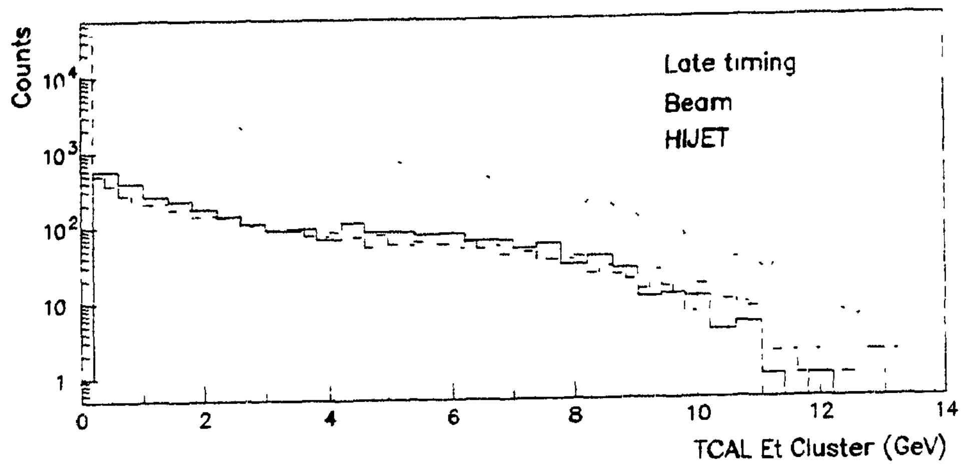

Figure 4.9 TCAL E_t as given by the beam trigger, the late timing trigger and HIJET.

[GR91].

Figure 4.9 also shows an E_t spectrum for charged particles calculated with HIJET. This spectrum is computed by tracking all the particles of 3000 Si + Pb events. The calculated E_t is computed with the same routine used to analyse the experimental data. One observes that the E_t spectrum calculated with HIJET is in good agreement with the minimum bias experimental spectrum. This confirms that the predictions of HIJET give a good description of the events in the target rapidity region. It also allows the use of the calculated E_t instead of the measured E_t to correct for the trigger bias.

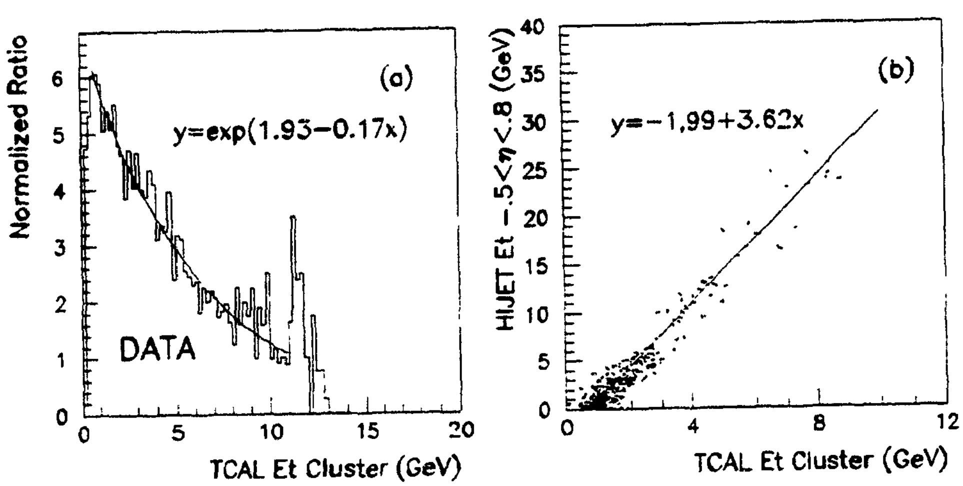

Figure 4.10 Trigger bias fits. (a) ratio of E_t spectra of the late timing trigger to the beam trigger. (b) Initial E_t from HIJET vs E_t measured in the TCAL with GEANT.

The following method is used to determine the trigger bias The ratio of the E_t spectra of late timing trigger to beam trigger is first calculated. This ratio is shown in figure 4.10(a). The ratio is fixed to 1 at E_t = 11 GeV The structure at E_t > 11 GeV is due to the limited statistics in that region. As expected, the ratio shows that the late timing trigger enhances, by a factor of up to 6, the events with low multiplicity This ratio can be described with an exponential function

$$w = \exp(1.93 - 0.17 \ E_t^{meas}) \tag{4.1}$$

where E_t^{meas} is the experimental transverse energy measured in the TCAL. As shown by the solid line in figure 4.10(a) this function gives a good representation of the observed trend.

Formula 4.1 provides a weighting factor which is a function of E_t^{meas} or the centrality of the event. To use formula 4.1 on an event by event basis, however, would require tracking complete events through the TCAL to determine E_t^{meas} This would be time consuming and most of the computer time would be spent on tracking particles that do not hit the silicon detector. Instead, we use the fact that there is a strong correlation between the E_t generated by HIJET and the E_t measured by the TCAL. This is shown in figure 4.10(b) which was generated with 2300 fully tracked events In this figure, the E_t generated by HIJET in the pseudorapidity range $-0.5 < \eta < 0.8$ is compared to the simulated E_t^{meas}.

The large factor (~ 4) between the raw E_t and the TCAL E_t comes from the fact that on average only $\sim 50\%$ of the energy of each particle hitting the TCAL is detected and furthermore, that the TCAL has gaps in its coverage [BA90A]. The relation between the E_t generated by HIJET and the E_t^{meas} is parametrized with a straight line fitted to the distribution of figure 4.10(b) [BE69]. By combining this relation and equation (4.1), the weighting factor is expressed as a function of E_t^{HIJET} instead of E_t^{meas} This weighting factor is given by :

$$w = \exp(1.823 - 0.052 \cdot E_t^{HIJET}). \tag{4.2}$$

By using relation (4.2), the weight of an event can be deduced without tracking all the particles through the TCAL. To simulate the trigger bias the weight correction given in formula (4.2), rounded of to the nearest integer, is applied to 3000 events which are completely tracked through the TCAL. As is shown in figure 4.11, the experimental E_t spectra obtained with the late timing trigger is well reproduced by the weighted simulation. This method of accounting for the trigger bias allows a substantial reduction in computer time and, on the average, is consistent with full tracking.

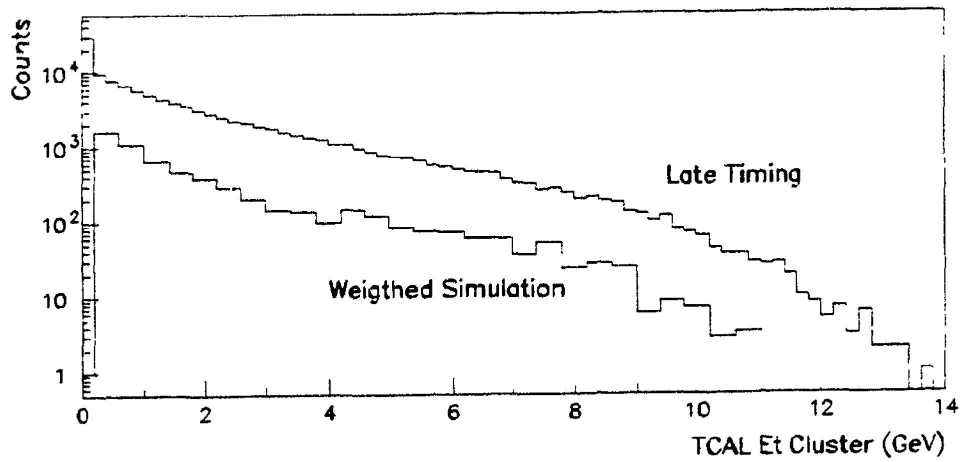

Figure 4.11 Trigger bias correction. The E_t spectra shapes obtained from the data is compared to the bias correction applied to HIJET.

4.4 Detailed simulation

In section 4.2 it was argued that a detailed simulation is necessary to properly study the detector response. The most accurate simulation requires full tracking of all particles of each event. However, because of the small solid angle covered by the silicon detector, most of the computer time would be spent on tracking particles that would not hit the detector. The silicon detector is centered on the top wall of the TCAL as shown in figure 2.2. Thus the contribution to the spectrum from the particles emitted in the direction of the other walls of the TCAL can be safely neglected. Only the particles generated toward the top wall were tracked i e., if their initial direction was within $48° < \theta < 118°$ and $40° > \phi > 140°$. For the present simulation, 14400 ^{28}Si + ^{208}Pb HIJET events were tracked by GEANT through the target, the silicon detector, the TPAD and the TCAL. From all the events that were tracked, 460 particles hit the silicon detector and out of these, 290 had a corresponding cluster in the TCAL. The calculation was done on a VAXstation 3200 computer and required ~ 4 days of cpu time. The events produced by HIJET are weighted to account for the experimental trigger bias.

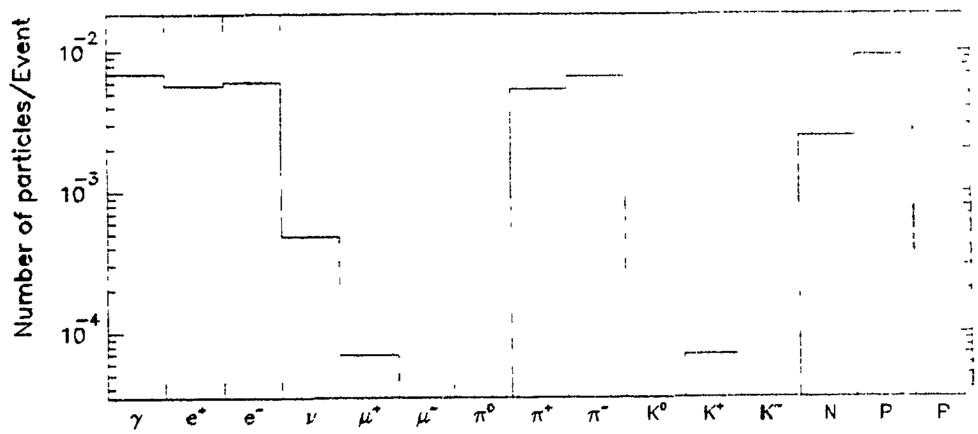

Figure 4.12 Types of particles that hit the silicon detector according to HIJET.

An inventory of the particle species that hit the silicon detector in this detailed simulation is presented in figure 4.12. The histogram is normalized to give the rate of hits in the silicon detector per event. This figure can be compared to the production rates of particles by HIJET in the same angular range presented in figure 4 2. As expected, all the π^0 have decayed into two γ rays. A fraction of these γ rays were converted into e^- and e^+ pairs through interactions in the target. Because of the thick target used during the present test (11.33 g/cm^2), on average, a particle goes through 1.5 cm of lead (2.7 radiation lengths) in the target before it reaches the silicon detector. The attenuation length for γ rays in lead above 100 MeV in energy is ~10 g/cm^2. Therefore, $\approx$ 60% of the γ convert in the target The particles generated by conversions are strongly correlated, thereby increasing the probability of double hits One notes that the yield of e^-, e^+, π^+ and π^- are all nearly equal One also notes that the predicted yield from for protons is ~ 1.5 times larger than for pions, since ~ 11 times more protons than pions are generated by HIJET (as shown in figure 4.2) this indicates that most of the produced protons are absorbed in the target According to this simulation, the contributions from other charged particles is negligible

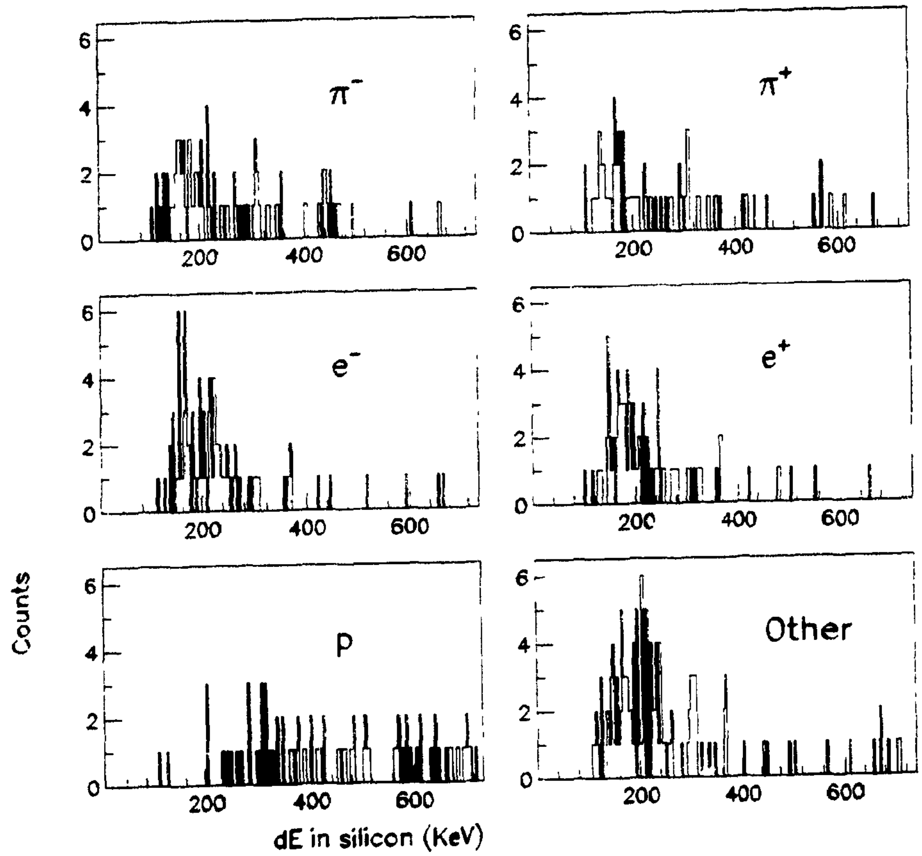

Figure 4.13 dE in the silicon according to the particle type by tracking a quarter of the particles.

The calculated energy loss distribution in the silicon detector is plotted in figure 4.13 for five types of particles: π^-, π^+, e^-, e^+ and p hitting the silicon detector. The sum of the contributions of other particles is also presented. Once the tracking is completed by GEANT, all the contributions are summed to get the total energy loss detected by the silicon detector. This is done on an event by event basis so that the effects of double hits are accounted for. Note that each corresponding histogram is incremented when the calculated signal is above pedestal for each particle that hits the silicon detector in a given event. The calculation indicates that most of the pions are minimum ionizing as are nearly all the electrons and positrons. This is consistent with the results obtained with the single particle simulations, shown in figure 4.4, where the corresponding histogram from electrons and positrons is labeled with the initial

π^0. Protons are not minimum ionizing and present a large rate of energy loss The distribution for other particles is very similar to that of electrons and positrons The entries of this histogram are mostly due to neutral particles that pass through the silicon detector in coincidence with charged particles The total spectra of energy loss in the silicon detector is shown in figure 4 14 This histogram is filled once per event and is thus different from the sum of the histograms of figure 4 13 Even with the low accumulated statistics, one observes that the shape of the calculated spectrum is in good agreement with the measured one shown by the dotted line

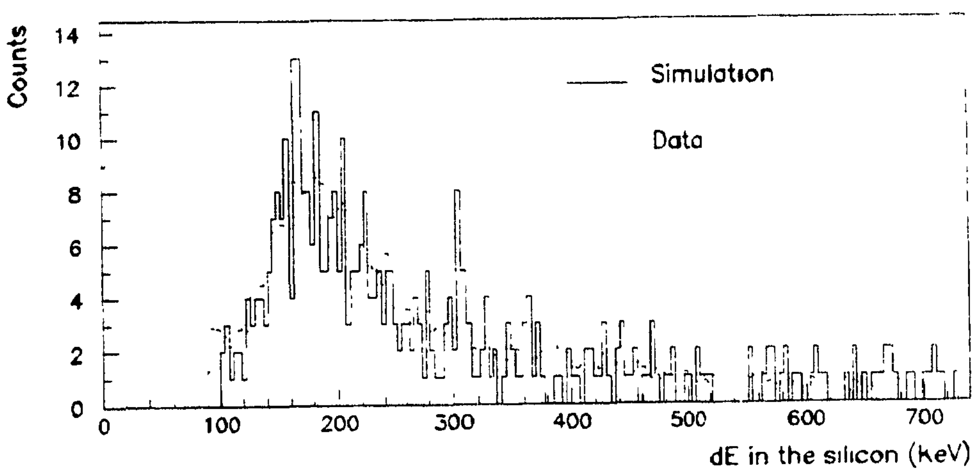

Figure 4.14 Total dE in the silicon as given by tracking a quarter of the particles.

The correlation between the energy loss measured in the silicon detector and the energy measured in the TCAL is shown in figure 4.15. For each type of particle, the histograms are filled when a signal above pedestal is seen by the silicon detector and a corresponding cluster is found in the TCAL. If more than one particle hits the silicon detector, the corresponding graph for each particle is filled and the energy used is the total energy seen in the two detectors. In the two first histograms of figure 4.15, one can see that the charged pions are grouped in roughly the same region of the graph as in the single particle simulation Most of them are minimum ionizing in both detectors and form a cloud around 0.1 GeV in the TCAL However, they are spread over a larger area than predicted by the single particle simulation. On the other hand, the e^- and e^+ form an horizontal band These histograms show that the e^-

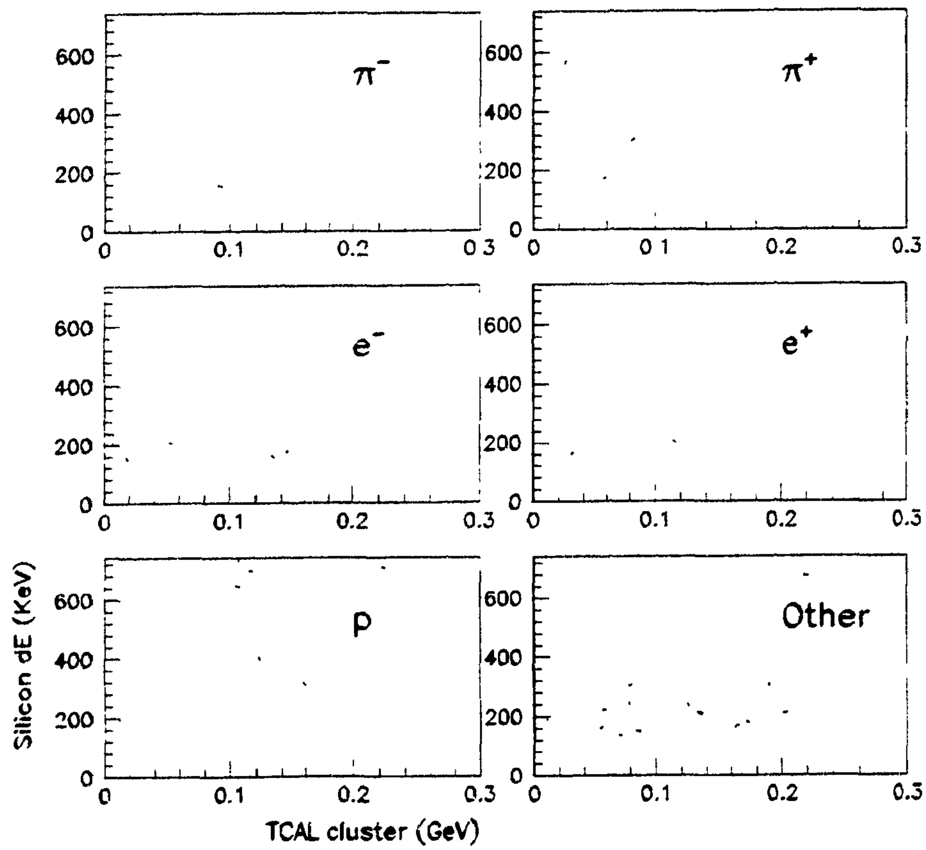

Figure 4.15 dE vs E according to the particle type by tracking a quarter of the particles.

and e^+ are minimum ionizing in the silicon detector but leave a large range of energy in the TCAL. In the case of protons, the results from this detailed simulation indicate that their distribution is structureless and very different from the one obtained in the calculation done with the single particle generator. They are spread over the top right portion of the histogram. The last graph of figure 4.15 is filled for the other types of particles. The main contribution to this graph comes from neutral particles that pass through the silicon detector in coincidence with charged particles like in figure 4.13.

Figure 4.16 shows the dE vs E correlation which is filled once per event using the total calculated energies for each detector in events where a cluster was found in any of the three TCAL crystals behind the silicon detector ((17,5), (17,6), (17,7)). This figure contrasts with the corresponding one obtained with the single particle generator that

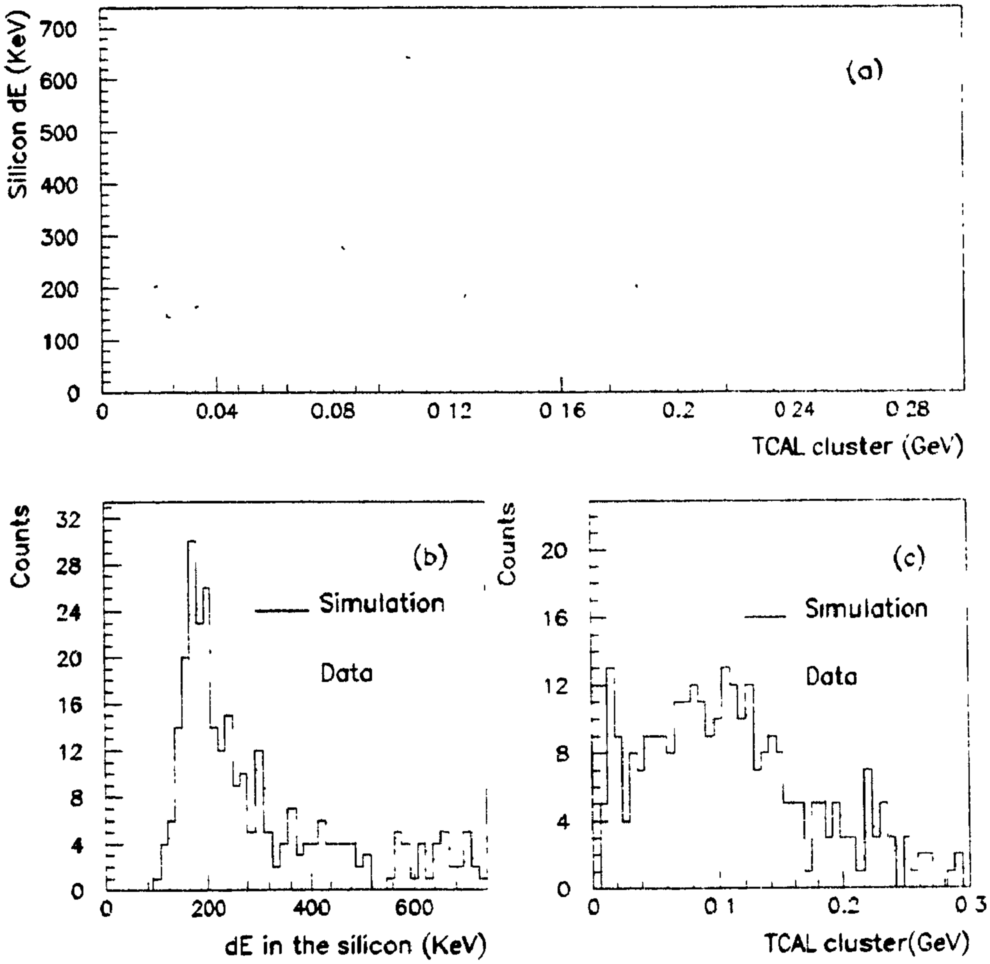

Figure 4.16 Total dE vs E by tracking a quarter of the particles (a) dE vs E matrix. (b) dE in the silicon detector. (c) Cluster energy measured in the TCAL.

is shown in figure 4.7. As it was apparent in the discussion of figure 4.15, no clear cut bands of pions or protons can now be identified. The calculated dE vs E scatter plot presented in figure 4 16 gives a fair representation of the experimental data shown in figure 3.9. In both cases, the density of particle peaks in the minimum ionizing region of the graph and a structureless decrease in the number of entries to the other regions of the histogram is observed.

The spectra corresponding to the projections on each axis of figure 4 16(a) are plotted in figure 4.16(b) and 4.16(c). The data are shown by dotted lines and scaled to the calculation for comparison. In spite of the limited statistics, one can see that the shape of the calculated energy loss spectra in the silicon detector (figure 4.16(b)) is in fair agreement with the data. However, one notes that the calculation systematically underestimates the high end of energy spectrum. The cluster energy distribution in the TCAL (figure 4.16(c)) is quite broad. The sharp peak at 0.08 GeV obtained in the calculation done with the single particle generator has completely disappeared in this more complete simulation The shape of the experimental cluster energy spectra (dotted line) is well reproduced from 0 1 GeV to 0.3 GeV. However, the calculated yield decreases at lower cluster energies contrary to the data.

The differences between the results from the detailed simulation and those obtained with the single particle generator have two main origins. The first one is attributable to the high probability of double hits in the TCAL as discussed in section 3 5 In the detailed simulation, all particles are tracked simultaneously to include the effects of the double hits in individual TCAL crystals. Moreover, the probability for two particles to hit adjacent TCAL crystals also become important; each crystal has eight immediate neighbors. This effect is also present in the measurements. The cluster finding routine of the TCAL can't separate two such particles and this affects the quality of the individual particle energy measurement of the TCAL. This causes a general smearing of the energy distributions as compared to the results obtained with the single particle generator. This explains the disappearance of the peak due to pions in the minimum ionizing part of the dE vs E has matrix. The cluster finding routine is used because the showers produced by particles in the TCAL are physically larger than the size of individual crystals. As a result, the effective granularity of the TCAL is considerably smaller than that of its crystals.

The second effect that explains the differences between the detailed simulation and the results obtained with the single particle generator is attributed to the large contribution of the electrons and positrons These two particles are minimum ionizing in the silicon detector. However, they leave a broad range of energy signals in the TCAL. In the present test, this constitutes an overwhelming background to the energy spectra measured by the TCAL. This effect could be reduced by using a thinner target. However, it will always be a limitation. in particular, in the characterization of reaction products having small production cross section and that necessitate the use of thick targets.

The detailed calculation presented in this section shows that the quality of a model independent identification of charged particles would be marginal with the simple addition of a silicon detector in front of the the E814 target calorimeter, in agreement with the data.

5

Conclusion

Simple simulations indicated a possibility of achieving particle identification at target rapidities in the upgraded E814 experimental setup. This could be done using an upgraded charged particle multiplicity silicon detector and the existing target calorimeter. A test was carried out to study the quality of particle identification achievable with such a multiplicity detector. The test was done using a silicon barrier detector and part of the target calorimeter. The experimental data were found to be very different from what was predicted by the simple simulations. Therefore, more detailed calculations were made to understand the response of the detectors.

A detailed simulation of the detectors using single particles indicated that the non-uniformities of the TCAL and the leakage between the crystals were important factors that affected the resolution of the individual particle energy measurement. However, the results obtained with the single particle generator are still in disagreement with the experimental data and predict better defined dE vs E distributions than observed. A more accurate simulation was done to completely understand the response of each detector. To include all possible effects as accurately as possible, the experimental trigger bias was parametrized by tracking complete events through the TCAL. The results from a final calculation, were shown to be in good general agreement with the data. Because of the horizontal extension of the showers in the TCAL is larger than the width of its crystals, the high probability of adjacent crystal hits was found to greatly reduce the resolution of the energy measurement for single particles. The contributions from e^+ and e^- from the conversion of γ-rays due to the decay of π^0

was also found to be an important background to the particle identification. From the results obtained with the last simulation, it was concluded that a model-independent particle identification was difficult with the simple addition of a silicon detector in front of the existing E814 target calorimeter.

The possibility of making a statistical particle identification using only the energy loss information of the silicon detector was also studied For this method to produce a reliable measurement it is necessary that no more than two types of particle contribute to the energy loss spectrum. However, the contributions from e^+ and e^- were found to be important. The energy loss spectra of e^+ and e^- were found to be similar to those of π^+ and π^-. Therefore, their respective contributions can be interchanged without affecting the shape of the total energy loss spectra This is confirmed by the fact that the calculated energy loss spectra from all the simulations are all consistent with one another even though the particle types involved are very different from one simulation to the other.

Since the simple approach tested in this thesis does not appear to provide a model-independent particle identification, it is likely that major modifications to the existing E814 setup would be required to reach a reasonable level of reliability. The use of a thick calorimeter, in particular, would permit a more accurate determination of the particle energy and help in the resolution of ambiguities The angular coverage of the calorimeter could be reduced in order to minimize contributions of shower overlaps and energy pileup. A longitudinal segmentation of the detector would also be helpful in providing an estimate of particle range and in the determination of particle species. Such a detector is now planned and will be part of an upgraded experimental setup that will be used to study reactions with heavy beams [Li91].

References

[AB87] T. Abbot et al., *Preliminary Results from Brookhaven Experiment 802*, Proc. IX Autumn School on the Physics of the Quark-Gluons Plasma, Lisbon, Portugal, (1987)

[AB90] T. Abbot et al , *Kaon and Pion production in central Si+Au collisions at 14.6 GeV/c*, Phys. Rev Lett., **64**, (1990)847.

[BA90A] J. Barrette et al., *Energy Flow and Stopping in Relativistic Heavy-Ion Collisions at E_{lab}/A=14.6 GeV*, Phys. Rev **C64**, (1990)1219.

[BA90B] J. Barrette et al., *Electromagnetic Dissociation of ^{28}Si at $E_{lab}/A = 14.6 GeV$ by Nucleon Emission*, Phys. Rev **C41**, (1990)1512.

[BA90C] J. Barrette et al., *Search for Strange Quark Matter in High Energy Heavy Ion Collision*, Phys. Lett. **B252**, (1990)550.

[BA91A] J. Barrette et al , *Forward Baryons in Relativistic Nucleus-Nucleus Collisions*, approved for publication in Phys Rev. C

[BA91B] J. Barrette et al., *Charged Particle Multiplicities in Relativistic Heavy Ion Collisions*, Submitted to Phys Rev. C

[BE69] P. R. Bevington, *Data Reduction and Error Analysis for the Physical Sciences*, McGraw Hill, USA, (1969)105.

[BR84] R. Brun et al., *GEANT3*, CERN Data Handling Division, DD/EE/84-1,(1984), unpublished.

[BR89] R. Brun et al., *PAW-Physics Analysis Workstation The complete Reference Version 1.07 (October 1989)*, CERN Program Library, Q121, (1989), unpublished

[DA91] G. David, E814 documentation and private communications

[DE63] G. Dearnaley and D C Northrop, *Semiconductor Counters for Nuclear Radiations*, E. & F.N. Spon, USA, (1963)221

[FA87] M. Fatygua et al , *Linear Momentum transfer and light particle emission in the $E/A = 25MeV\ ^6Li + ^{238}U$ Reaction*, Phys. Rev **C35**, (1987)568.

[FA91] M. Fatygua, D Makowiecki and W Llope, *Fast Monte Carlo Simulation of Segmented U/Cu/Scint Calorimeters*, Nucl Instr and Meth , **A284**, (1991)323

[FR89] B.L. Friman, *Strangeness in ultra-relativistic heavy-ion collisions*, Quark Matter '88, Nucl. Phys., **A498**, (1989)161c

[GO75] F.S. Goulding and B.G Harvey, Ann. Rev Nucl. Sci., **25**, (1975)167

[GO79] F.S. Goulding, *Ion Identification With Detector Telescopes*, Nucl. Inst. and Meth , **A162**, (1979)609.

[GR91] V.S. Green, , Ph.D. Thesis, York University, (1991), to be submitted.

[HE90] J.J. Hernández et al., *Review of Particle Properties*, Phys. Lett **B239**, (1990)III

[JA89] M. Jacob, *Quark Matter – Facts and Hopes*, Quark Matter '88, Nucl. Phys., **A498**, (1989)1c.

[LE87] W.R. Leo, *Techniques for Nuclear and Particle Physics Experiments*, Springer-Verlag, Germany, (1987)57.

[LI86] D. Lissauer et al., *Proposal 814 submitted to the AGS Program Committee*, BNL, (1986), unpublished.

[LI91] D. Lissauer et al., *Proposal 877 submitted to the AGS Program Committee*, BNL, (1991), unpublished

[LU85] T. Ludlam, A. Pfoh, and A. Shor, *A Monte Carlo Event Generator for p-Nucleus and Nucleus-Nucleus Collisions*, Proceedings RHIC Workshop I, ed. P. Haustein and C. Woody, BNL-51921. (1985)373

[MA87] T Matsui and H.Satz, Phys. Lett , **B178**, (1986)416.

[NA88] S Nagamiya, *Toward new forms of nuclear matter with Relativistic Heavy Ion collisions*, Nucl. Phys., **A488**, (1988)3c.

[PA82] F.E Paige and S D. Protopopescu, *ISAJET· A Monte Carlo Event Generator for pp and $p\bar{p}$ Interactions*, Proc. 1982 DPF Summer Study on Elementary Particle Physics and Future Facilities,(1982).

[RA82] J. Rafelski and B Müller. *Strangeness Production in the Quark Gluon Plasma*, Phys. Rev Lett., **42**, (1982)1066.

[SA89] H. Satz, *J/ψ suppression in nuclear collisions· deconfinement of absorption?*, Quark Matter '88. Nucl. Phys., **A498**, (1989)495c.

[SH89] A. Shor and R. Longacre, *Effects of Secondary Interactions in Proton-Nucleus and Nucleus-Nucleus Collisions Using the HIJET Event Generator*, Phys. Lett. **B218**, (1989)100.

[SK89] W. Skulski et al., *Emission of Energetic Protons at Backward Angles in Central Collisions*, Phys Lett., **B218**, (1989)7.

[ST91] J. Stachel, *Systematics of global observables in relativistic heavy ion collisions*, Quark Matter '90, Nucl. Phys., **A525**, (1991)23c.

[TA91] H. Takai, E814 documentation and private communications.

[TE90] *Instruction Manual Silicon Surface Barrier Detector*, TENNELEC, (1990).

[TI88] M. Tincknell, *Transverse Energy in Nucleus-Nucleus Collisions, A Review*, Hadronic Matter in Collision 1988, Ed. P. Carruthers and J. Rafelski, World Scientific, Singapore, (1989)378.

[WA90] L. Waters, *Energy flow in relativistic heavy ion collisions at AGS*, Ph.D. Thesis, State University of New York at Stony Brook, (1990)

[WI84] E. Witten, *Cosmic separation of phases*, Phys. Rev., **D30**, (1984)272